UNANNOUNCED

PHOTOGRAPH THIS SHEET

DTIC FILE COPY

AD-A955 975

DTIC ACCESSION NUMBER

LEVEL

1

INVENTORY

AFAL-TR-72-226 Vol I

DOCUMENT IDENTIFICATION

OCT 1972

DISTRIBUTION STATEMENT A

Approved for public release;
Distribution Unlimited

DISTRIBUTION STATEMENT

ACCESSION FOR

NTIS GRA&I

DTIC TRAC

UNANNOUNCED

JUSTIFICATION

BY

DISTRIBUTION/

AVAILABILITY CODES

DISTRIBUTION	AVAILABILITY AND/OR SPECIAL	
A-1		

DISTRIBUTION STAMP

DTIC
ELECTE
OCT 03 1990
S D
E

DATE ACCESSIONED

QUALITY INSPECTED 4

UNANNOUNCED

DATE RETURNED

90 09 28 006

DATE RECEIVED IN DTIC

REGISTERED OR CERTIFIED NUMBER

PHOTOGRAPH THIS SHEET AND RETURN TO DTIC-FDAC

DTIC FORM 70A APR 87

DOCUMENT PROCESSING SHEET

PREVIOUS EDITIONS MAY BE USED UNTIL STOCK IS EXHAUSTED

AFAL-TR-72-226
Volume I

TARGET SIGNATURE ANALYSIS CENTER: DATA COMPILATION

ELEVENTH SUPPLEMENT

Volume I

Bidirectional Reflectance: Definition, Discussion, and Utilization

Prepared by

Target Signature Analysis Center
Infrared and Optics Division
Willow Run Laboratories
The University of Michigan
Ann Arbor, Michigan

October 1972

Air Force Avionics Laboratory
Air Force Systems Command
Wright-Patterson Air Force Base, Ohio

NOTICES

Note. When Government drawings, specifications, or other data are used for any purpose other than in connection with a definitely related Government procurement operation, the United States Government thereby incurs no responsibility nor any obligation whatsoever: and the fact that the Government may have formulated, furnished, or in any way supplied the said drawings, specifications, or other data is not to be regarded by implication or otherwise as in any manner licensing the holder or any other person or corporation or conveying any rights or permission to manufacture, use, or sell any patented invention that may in any way be related thereto.

Final Disposition. After this document has served its purpose, it may be destroyed. Please do not return it to the Willow Run Laboratories.

TARGET SIGNATURE ANALYSIS CENTER: DATA COMPILATION

ELEVENTH SUPPLEMENT

Volume I

Bidirectional Reflectance: Definition, Discussion, and Utilization

Prepared by

Target Signature Analysis Center
Infrared and Optics Division
Willow Run Laboratories
The University of Michigan
Ann Arbor, Michigan

FOREWORD

The work reported herein, covering the period from 1 November 1969 to 30 July 1972, was carried out by the Infrared and Optics Division of the Willow Run Laboratories, a unit of The University of Michigan's Institute of Science and Technology, Ann Arbor, Michigan. The work was performed under Contract F33615-70-C-1123, Project 6239, Task 10, for the Air Force Avionics Laboratory (AFAL), Air Force Systems Command, Wright-Patterson Air Force Base, Ohio. Volume I contains a definition of the parameters pertinent to the bidirectional reflectance, a discussion of the data, some equations for application of the data, and an index and cross reference of the data contained in Volume II. Bidirectional reflectance data in graphical form are presented in Volume II. The data were reduced and this supplement was prepared by (Mrs.) Sharon Ladd, Dwayne Carmer, Daniel Rice, Dennis Ladd, and John Ulrich under the direction of J. Robert Maxwell. The data reported in this supplement were obtained almost entirely from the laboratory measurements phase of the Target Signature Measurement Program conducted at The University of Michigan, sponsored by the Avionics Laboratory under U. S. Air Force Contracts AF33(615)-3924, F33(615)-68-C-1281 and F33(615)-70-C-1698, under the direction of Max Bair.

The Target Signature program is part of a comprehensive multispectral program at The University of Michigan devoted to the improvement of remote sensing capabilities; this comprehensive program is under the supervision of R. R. Legault, Associate Director of the Willow Run Laboratories. The Principal Investigator for this contract is J. R. Maxwell. The Willow Run Laboratories' number for this report is 32210-41-B (I and II).

This report was submitted by the authors on 10 August 1972.

This technical report has been reviewed and is approved.

D. ROGER SINK, ACTING CHIEF
Reconnaissance Applications Branch
Reconnaissance Division
Air Force Avionics Laboratory

ABSTRACT

This report is the eleventh supplement to the Target Signature Analysis Center: Data Compilation and contains 2200 curves of bidirectional reflectance versus angle. The significance of this report to the Air Force is that these data provide the Air Force with essential optical properties-of-materials data to analyze the angular dependence of the reflected radiance from various targets. Volume I contains a definition of the parameters pertinent to the bidirectional reflectance, a discussion of the data, some equations for application of the data, and an index and cross reference of the data contained in Volume II. Bidirectional reflectance data are presented graphically in Volume II.

This supplement to the Target Signature Analysis Center: Data Compilation augments an ordered, indexed compilation of reflectance, radar cross sections, and apparent temperatures of target and background materials. The Data Compilation includes spectral reflectances and transmittances in the optical region from 0.3 to 15 μm, normalized radar cross sections, and apparent temperatures at mm wavelengths. When available, the experimental parameters associated with each curve are listed to provide the user with a description of the important experimental conditions.

CONTENTS

FIGURES

TARGET SIGNATURE ANALYSIS CENTER: DATA COMPILATION
ELEVENTH SUPPLEMENT

Volume I

1
INTRODUCTION

The development of improved reconnaissance and weapon guidance sensors requires a better knowledge of target and background signatures. The sensor designer has many sensor parameters to consider in his tradeoff studies, and he must have the radiation characteristics of a variety of targets and backgrounds under a wide variety of environmental conditions to design a sensor which will meet the Air Force's operational measurements. The Target Signature Analysis Center (TSAC) at the Willow Run Laboratories (WRL), under sponsorship of the Air Force Avionics Laboratory, provides the necessary optical properties-of-materials data and analytical programs which: (1) compute surface temperatures for emission analyses; (2) compute the spectral and spatial distribution of sky illumination for reflection by the target; (3) treat the geometrical properties of the target and all of the angular, spectral, and polarization characteristics of the reflectance and emittance properties of the materials which constitute the target; and (4) account for absorption, scattering, and emission by the atmosphere between the target and the sensor.

The Target Signature Analysis Center: Data Compilation* includes spectral reflectances, transmittances, and emittances in the optical region from 0.3 to 15 μm, normalized cross sections, and apparent temperatures at millimeter wavelengths. The reflectances of many target and background materials depend strongly on the positions and polarizations of the source and receiver in addition to the wavelength of the source. These dependences are very important for the analyses of radiance characteristics from targets/backgrounds at a remote sensor.

Bidirectional reflectance data have been collected and reduced, and 2200 curves are presented in this supplement to the Target Signature Analysis Center: Data Compilation. Volume I contains a definition of the bidirectional reflectance and its spectral and source/receiver angular and polarization dependence, a discussion of the data, some equations for application of the data, and an index and cross reference of the data contained in Volume II. Bidirectional reflectance data are presented graphically in Volume II.

*The original Data Compilation and the first ten supplements are listed in Appendix I.

2
BIDIRECTIONAL REFLECTANCE

The reflectance of a surface generally depends on the aspect angle of the source, its polarization and wavelength, and on the viewing angle of the receiver with polarizations generally modified when reflection occurs. The bidirectional reflectance is a complete specification of these reflectance characteristics. It is defined as the ratio of the radiance reflected by the sample in the direction of the receiver, (θ_r, ϕ_r), to the irradiance incident on the sample from direction (θ_i, ϕ_i). The wavelength of the source, its polarization, and the polarization of the reflected radiance are important parameters. The complete plane-polarized bidirectional reflectance, $\rho'_{\alpha i,\alpha r}(\lambda; \theta_i,\phi_r; \theta_r,\phi_r)$, is*

$$\rho'_{\alpha i,\alpha r}(\lambda; \theta_i,\phi_i; \theta_r,\phi_r) = \frac{L^r_{\alpha r}(\theta_r, \phi_r)}{E^i_{\alpha i}(\theta_i, \phi_i)} = \frac{\text{reflected W/cm}^2\cdot\text{sr}}{\text{incident W/cm}^2} \qquad (1)$$

where $E^i_{\alpha i}(\theta_i, \phi_i)$ is the irradiance on the sample from direction (θ_i, ϕ_i), and $L^r_{\alpha r}(\theta_r, \phi_r)$ the radiance reflected in direction (θ_r, ϕ_r). The wavelength of the incident irradiance is denoted by λ. The subscripts αi and αr represent, respectively, the plane-polarization state of the incident irradiance and the plane-polarized component of the reflected radiance selected by the polarization analyzer on the receiver. The polarization azimuth angles αi and αr represent the orientation angles for the polarizers on the source and receiver respectively. The geometrical variables are shown in Fig. 1 and the angle between (θ_i, ϕ_i) and (θ_r, ϕ_r) is the bistatic angle which is denoted by 2β.

The polarization specifier known as the polarization azimuth angle, α, is the angle between the electric field polarization plane and the normal vector to the reference plane. Thus, $\alpha = 0$ corresponds to perpendicular polarization. The polarization azimuth angle is constrained to satisfy $-90 \le \alpha \le 90$. The sign is determined by a viewer looking into the propagating radiation (i.e., looking "upstream"). If the angle <u>from</u> the reference-plane normal vector <u>to</u> the electric field polarization plane is counterclockwise for such a viewer, then the polarization azimuth angle is positive.

---

*In the present discussion, the bidirectional reflectance is denoted formally by ρ' and given the verbal name "rho-prime." Other formal notations in common use, including use in previous Data Compilation Supplements, are $\acute{\rho}$, f_4, and 4RDF. ρ' has been selected here as being the last-objectionable of these notations.

According to rules set down in 1970 by the CIE in Ref. [1], the most appropriate symbol would be ρ_Ω. However, that symbol is not seriously suggested here because there are already too many symbols in common use and ρ_Ω has not actually been used before.

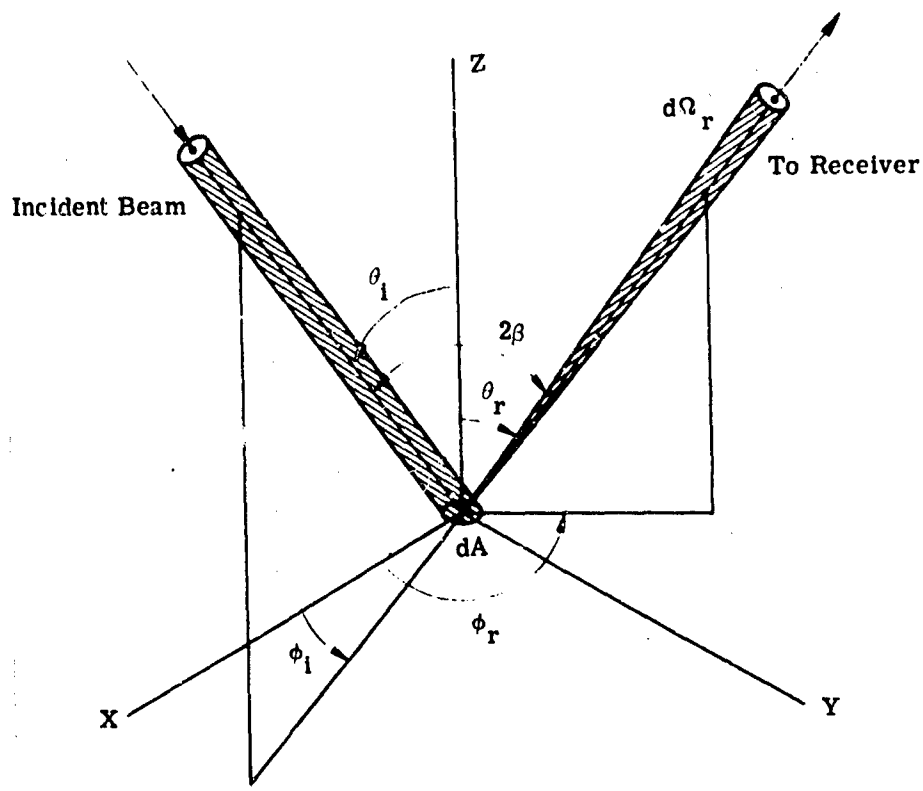

FIGURE 1. BIDIRECTIONAL REFLECTANCE GEOMETRICAL PARAMETERS. The coordinate origin is on the surface of the sample and the Z-axis is perpendicular to that surface. The azimuth reference (X-axis) is arbitrary. The zenith angles are constrained to lie between 0 and $\pi/2$, the azimuth angles between 0 and 2π, and the bistatic angle between 0 and π.

The polarization indicators used on the data reported in this Supplement are $\perp$ and $\parallel$ ($\alpha = 0$ and 90, respectively). If the incident irradiance is unpolarized, the symbol αi in Eq. (1) is replaced with U. If the detector used in a ρ' measurement has no polarization preference and senses the total radiance at the receiver aperture, the symbol αr in Eq. (1) is replaced by T. Thus, for example, $\rho'_{\perp,\perp}$ represents the result of a measurement under conditions of perpendicularly-polarized sample irradiance and a perpendicularly-polarized analyzer on the receiver. The symbol $\rho'_{U,T}$ refers to conditions of unpolarized incident irradiance and no analyzer on the receiver.

Manipulation of Eq. (1) leads to many interrelationships of the bidirectional reflectance distributions for various polarization states of $E^i_{\alpha i}$ and $L^r_{\alpha r}$. The most fundamental ones are

$$\rho'_{\perp,T} = \rho'_{\perp,\perp} + \rho'_{\perp,\parallel}$$

$$\rho'_{\parallel,T} = \rho'_{\parallel,\parallel} + \rho'_{\parallel,\perp}$$

$$\rho'_{U,\perp} = \frac{1}{2}(\rho'_{\perp,\perp} + \rho'_{\parallel,\perp}) \qquad (2)$$

$$\rho'_{U,\parallel} = \frac{1}{2}(\rho'_{\parallel,\parallel} + \rho'_{\perp,\parallel})$$

$$\rho'_{U,T} = \frac{1}{2}(\rho'_{\perp,\perp} + \rho'_{\perp,\parallel} + \rho'_{\parallel,\parallel} + \rho'_{\parallel,\perp})$$

If reciprocity is invoked (Ref. 2)

$$\rho'_{\alpha i,ar}(\lambda;\ \theta_i,\phi_i;\ \theta_r,\phi_r) = \rho'_{\alpha r,\alpha i}(\lambda;\ \theta_r,\phi_r;\ \theta_i,\phi_i) \qquad (3)$$

which says that the results of the following two ρ' measurements are the same; namely, ρ' with the source at (θ_i, ϕ_i) with a polarizer αi and receiver at (θ_r, ϕ_r) with analyzer αr, and ρ' with the source at (θ_r, ϕ_r) and polarizer αr and receiver at (θ_i, ϕ_i) with analyzer αi.

The directional reflectance data which have been previously published in the Data Compilation represent a measurement of the ratio of the total power reflected (into the entire hemisphere) by a sample to the power incident on the sample. It is usually measured as a function of the wavelength, λ. Even though the angular effects are largely averaged out, these data are of major importance because of the spectral information they provide. For a measurement of directional reflectance, the incident power is unpolarized, spectrally filtered in a wavelength band $\Delta\lambda$ centered at wavelength λ, collimated, and directed onto the sample at an angle of incidence (θ_i, ϕ_i). The directional reflectance, $\rho_d(\lambda;\theta_i,\phi_i)$ is then a bidirectional reflectance averaged over (θ_r, ϕ_r) and is related to the bidirectional reflectance as follows. With an unpolarized irradiance on the sample $E^i_U(\theta_i, \phi_i)$, the radiance reflected in direction (θ_r, ϕ_r), $L^r_T(\theta_r, \phi_r)$, is given by the expression

$$L^r_T(\theta_r, \phi_r) = \rho'_{U,T}(\lambda;\ \theta_i,\phi_i;\ \theta_r,\phi_r)E^i_U(\theta_i, \phi_i)$$

The power reflected by the sample of area A into an increment of solid angle $d\Omega_r$, $dP_T^r(\theta_r, \phi_r)$, is given by the expression

$$dP_T^r(\theta_r, \phi_r) = L_T^r(\theta_r, \phi_r) \cos \theta_r \, d\Omega_r A$$

The power reflected into the entire hemisphere P_T^r is

$$P_T^r = E_U^i(\theta_i, \phi_i) A \int_{2\pi} \rho'_{UT}(\theta_i, \phi_i; \theta_r, \phi_r) \cos \theta_r \, d\Omega$$

The unpolarized power incident on the sample from direction (θ_i, ϕ_i), $P_U^i(\theta_i, \phi_i)$, is

$$P_U^i(\theta_i, \phi_i) = E_U^i(\theta_i, \phi_i) A$$

Hence, the ratio of the power reflected into the entire hemisphere to the unpolarized power incident on the sample is

$$\frac{P_T^r}{P_U^i(\theta_i, \phi_i)} = \rho_d(\lambda; \theta_i, \phi_i) = \int_{2\pi} \rho'_{U,T}(\lambda; \theta_i, \phi_i; \theta_r, \phi_r) \cos \theta_r \, d\Omega_r \qquad (4)$$

The directional reflectance data do not provide any information about the angular distribution of the radiance reflected by the surface and are completely adequate only for surfaces for which $\rho'(\lambda; \theta_i, \phi_i; \theta_r, \phi_r)$ is independent of θ_r and ϕ_r. Usually $\rho_d(\lambda; \theta_i, \phi_i)$ is measured for one angle of incidence only, usually for $\theta_i = 0$ or 5 deg; the dependence on θ_i and ϕ_i is generally ignored and $\rho_d(\lambda; \theta_i, \phi_i) = \rho_d(\lambda)$ is assumed. Surfaces for which $\rho' = \rho'(\lambda)$ only are diffuse reflectors, and for a diffuse reflector $\rho'_{UT}(\lambda) = \rho_d(\lambda)/\pi$ and $\rho'_{\alpha i, \alpha r}(\lambda) = \rho_d(\lambda)/2\pi$. Diffuse reflectors with $\rho_d = 1$ are Lambertian.

It is important to emphasize that even though real surfaces depart markedly from being diffuse reflectors, the $\rho_d(\lambda)$ data are extremely valuable because, for many surfaces, the angular dependence of the bidirectional reflectances measured at one wavelength can be scaled to another wavelength with the directional reflectance data for wavelengths not too widely separated (e.g., 0.63 to 1.06 μm), i.e.:

$$\frac{\rho'(\lambda_1; \theta_i, \phi_i; \theta_r, \phi_r)}{\rho'(\lambda_2; \theta_i, \phi_i; \theta_r, \phi_r)} = \frac{\rho_d(\lambda_1)}{\rho_d(\lambda_2)}$$

This relationship has been found to be reasonably valid, except when the source and receiver are near the specular geometry, namely $\theta_r = \theta_i$ and $\phi_r = \phi_i + 180$.

3
INSTRUMENTATION AND DATA-REDUCTION PROCEDURES

An automated gonioreflectometer was designed and has been used to measure bidirectional reflectances as a part of the laboratory phase of the Target Signature Measurements Program conducted at Willow Run. A brief description of the instrumentation and the measurement- and data-reduction procedures is provided here to give a better understanding of the data presented in Volume II. More details are available in Refs. [3 and 4].

The automated gonioreflectometer facility is shown in Fig. 2. The sample is placed on the five-axis positioner. The sample may be moved relative to the source and receiver, or the sample may be placed in a fixed position relative to the source, with the receiver scanned in angle above the sample. All five axes are driven with dc motors and provide axis-position information to ±0.05 deg by synchro and dial indicators. A digital shaft encoder provides angular-position information at intervals between 0.1 deg and 8 deg.

For fairly diffuse samples for which the reflectance distribution is relatively constant, data can be taken at the rate of 15 points/sec which, at the fastest detector scan rate, corresponds to 2.5 points/deg of arc. Data on more specular samples cannot be taken as rapidly, since the higher frequency content of the changing signal levels will not pass through the processor. A typical data set at one wavelength, containing 4 polarization components on a given sample, could consist of 5 source incidence angles, detector scans in 4 azimuth planes from $\theta_r = 0$ to 80 deg, and 1 point for every 2 deg of arc of the scanning axis. Total time to acquire these 3200 data points is, including setup time, about 2 days.

Four illumination sources have been installed as component parts of the gonioreflectometer facility. Three continuous-wave (CW) laser sources provide linearly polarized sample illumination at wavelengths of 0.6118, 0.6328, 1.06, 1.15, 3.39, and 10.6 μm. A 1000-W tungsten-quartz-iodine lamp provides radiation in the 0.35- to 2.0-μm spectral range. Wavelength selection from the tungsten lamp is accomplished by use of narrowband filters at selected wavelengths in this range. Each radiation source is mounted on a concrete block table positioned on an 8-ft radius around the five-axis positioner. Each source has collimating optics and calibrated attenuators to control beam divergence and the size and intensity of the illumination on the sample. Source power is continuously monitored with a detector below a beamsplitter in the laser beam.

Three detector-optics assemblies have been designed and fabricated to provide receiver capabilities over the 0.4- to 14-μm spectrum. The detectors (a photomultiplier with an S-1 surface, a pyroelectric, and an InSb detector) and associated optics are mounted as integral units and can be easily interchanged on the receiver mounting boom. Each receiver package contains a linear polarization analyzer. In each instance, the field of view at the sample surface exceeds the area illuminated, and calibration is thereby simplified.

FIGURE 2. AUTOMATED GONIOREFLECTOMETER WITH TWO OF THE SOURCES

Calibration of the instrument is accomplished in the following manner. A calibrated neutral-density filter of sufficient density is placed between the source and the receiver, and a signal proportional to the incident power is obtained. To insure good calibration values, such calibrations are repeated at half-hour intervals or before and after each run. The output from the detector below a beam splitter in the laser beam monitoring the laser power is then adjusted so that it is equal to the calibration signal obtained in the detector channel when the detector views the source through an optical attenuator. The detector and monitor signals are both digitized and recorded on punched paper tape at specified angle increments controlled by the output of the digital shaft encoder. A CDC 1604 B digital computer programmed to read the paper tape then computes the bidirectional reflectance from the following equation:

$$\rho'(\theta_i, \phi_i; \theta_r, \phi_r) = \frac{V_r(\theta_r, \phi_r)K_r}{V_M K_c K_{NDF} \Omega_r \cos \theta_r} \tag{5}$$

where $V_r(\theta_r, \phi_r)$ = the voltage from the receiver at (θ_r, ϕ_r) caused by reflected power

K_r = precision electronics attenuator setting used for measurement of the voltage V_r

V_M = the monitor voltage (set equal to the calibration voltage at each calibration and sensitive to changes in laser power output between calibrations)

K_c = the electronic attenuator setting used for measurement of the voltage V_M

K_{NDF} = the attenuation of the calibrated neutral density filter used during the calibration measurement

Ω_r = the projected solid angle of the receiver as seen from the sample surface (about 0.0003 sr)

Most of the bidirectional reflectance data have been measured to within an accuracy of $\Delta\rho' = \pm 0.015\ sr^{-1}$. The $\Delta\rho'$ associated with large values of measured ρ' (i.e. ρ' greater than 0.3 sr^{-1}) is approximately, $\Delta\rho'/\rho' = 5\%$. At aspect angles greater than 45 deg, the measurements are less accurate. The precision is $\Delta\rho' = 0.005\ sr^{-1}$. Digital processing reduces the precision when highly reflecting samples are measured.

As an internal consistency check on the bidirectional and directional reflectance measurements made under the laboratory phase of the Target Signature Measurements program, measured bidirectional reflectance data at 0.63 and 1.06 μm have been integrated and compared with the directional reflectance at the same wavelengths. The comparison shows a 5% variation at most, and is within 2% to 3% in most cases.

In order that measured values of ρ' will represent optical properties of samples as opposed to characteristics of the measuring devices, certain precautions have been taken. The receiver aperture is small to obtain good angular resolution ($\Omega_r = 0.0003$ sr). The overall system signal-to-noise ratio sets the lower limit on the size of the aperture, since there are practical upper limits on the source power available. However, a lower-limit restriction on the receiver aperture is imposed when a highly coherent source (e.g., a laser) is being used, because it is

usually desirable to have the receiver aperture subtend many speckles in the coherent scattered field. The area illuminated on the sample, at normal incidence, is about 3/4 in. in diameter, large enough to contain a representative portion of the sample and small enough to ensure that θ_r does not undergo significant variation from point to point on the sample.

4
DISCUSSION OF THE DATA

4.1. ORGANIZATION

The ρ' data are presented graphically in Volume II on a logarithmic scale versus a linear scale for the angle variable. All data values on the graphs which are encircled should be multiplied by 100 to obtain the measured ρ' value. Usually four angle scans are given on each plot corresponding to $\rho'_{\perp,\perp}$, $\rho'_{\perp,\parallel}$, $\rho'_{\parallel,\perp}$, and $\rho'_{\parallel,\parallel}$. The legend at the top of each data sheet provides a key relating the source/receiver polarization code to the symbol on the curve. A shorthand notation has been used to indicate the polarization codes: $\perp\perp$ = X is the code and symbol for $\rho'_{\perp,\perp}$; $\perp\parallel$ = Δ the code and symbol for $\rho'_{\perp,\parallel}$, $\parallel\perp$ = + is the code and symbol for $\rho'_{\parallel,\perp}$, and $\parallel\parallel$ = ○ is the code and symbol for $\rho'_{\parallel,\parallel}$. The alphanumeric group of nine symbols at the top left of each graph is an identification number assigned to each sample by the Target Signature Analysis Center.* Additional sample information is available from TSAC to qualified users on request through the Air Force Avionics Laboratory, Wright-Patterson Air Force Base, Ohio.

The usual data-collection procedure is to scan the receiver in a fixed azimuth plane ($\phi_r = \phi_i$ or $\phi_r = \phi_i + 180$ for an in-plane θ_r scan; $\phi_r = \phi_i + 90$ or $\phi_r = \phi_i + 270$ for an out-of-plane θ_r scan) with the source at a fixed position, (θ_i, ϕ_i). Scans are usually made to obtain four polarized bidirectional reflectances, $\rho'_{\perp,\perp}$, $\rho'_{\perp,\parallel}$, $\rho'_{\parallel,\perp}$ and $\rho'_{\parallel,\parallel}$. Data are then obtained at several (θ_i, ϕ_i), and perhaps at several wavelengths.

Additional measurements are usually made with the bistatic angle, 2β, between the source and receiver fixed at some small angle, e.g. 1 or 2 deg. The sample is rotated about an axis contained in the plane of the sample to effect an angular scan in which the source and receiver are being simultaneously scanned as a rigidly connected pair. These angular scans are referred to as fixed bistatic-angle scans.

Occasionally data are obtained with the bistatic angle fixed at 1 or 2 deg with the sample rotated about the normal to the sample. These data are good indicators of the azimuthal asymmetry of the sample. They are also fixed bistatic-angle scans, but they are referred to as azimuth scans.

*The letter "A" in the sample number indicates that measurements on the sample were made at WRL. The letter "B" indicates that the data were taken and published by some other agency.

The data presented in Volume II are organized first according to sample material type. Eight material types and one category for miscellaneous are used. Specifically, with an approximate curve count, these material types are

(1) paint (1180 curves)
(2) cloth and canvas (400 curves)
(3) wood (110 curves)
(4) soil (25 curves)
(5) vegetation (50 curves)
(6) asphalt and concrete (50 curves)
(7) reflectance standards material (200 curves)
(8) metal (70 curves)
(9) miscellaneous (15 curves)

Within each of the above categories, the data are presented serially by sample number. For each specific sample, the data are presented in order of increasing wavelength. At any specific wavelength, the data are given in the following order:

(1) constant bistatic angle scans
(2) θ_r scans for $\phi_r = \phi_i$ and $\phi_r = \phi_i + 180$ (in-plane θ_r scans)
(3) θ_r scans for $\phi_r = \phi_i + 90$ and $\phi_r = \phi_i + 270$ (out-of-plane θ_r scans)
(4) θ_i scans
(5) azimuth scan

Only some of the above-listed data are available for any one sample.

In Section 7 of this volume, the Summary Catalog of the Data, some cross-referencing has been done. For example, sample number AO 1684, flame-sprayed aluminum, is listed under Reflectance Standards Material and cross-referenced under Metals.

4.2. DISCUSSION AND PERTINENT OBSERVATIONS

The number of bidirectional reflectance measurements which, in principle, are needed to completely specify the angular, polarization, and spectral properties of even just one sample is very large. The data in Volume II for any particular sample cover only a limited range of source and receiver positions, polarizations, and wavelengths. However, a number of trends

and characteristics are observed in these data. Some of these are useful for extrapolating the available measurements to other (λ; θ_i,ϕ_i; θ_r,ϕ_r) and for the development of empirical bidirectional reflectance models to extend the range of the data to all source/receiver positions, polarizations, and wavelengths. Others suggest possible discriminants between various materials over and above the spectral reflectance characteristics reported in earlier Data Compilation.

4.2.1. O.D. PAINT SPECULARITY

A characteristic common to much of the O.D. paint data at 0.63 and 1.06 μm is its pronounced specularity. An example is shown in Fig. 3. The source angle of incidence is 20 deg, i.e. (θ_i, ϕ_i) = (20, 0). The receiver is scanned in the plane of incidence from 0 deg to 80 deg in the backscatter (ϕ_r = 0) and forward scatter (ϕ_r = 180) azimuth planes. The $\rho'_{\perp,\perp}$ and $\rho'_{\parallel,\parallel}$ components are very large at the specular angle, (θ_r, ϕ_r) = (20, 180), and significantly smaller away from the specular angle. The $\rho'_{\parallel,\perp}$ and $\rho'_{\perp,\parallel}$ components, with source and receiver cross polarized, are small for all receiver angles. Data for the same sample with the source at (θ_i, ϕ_i) = (60, 0) are shown in Fig. 4, in which the specularity is again very pronounced but with the significant difference that the $\rho'_{\parallel,\parallel}$ component is much smaller at the specular angle. This is apparently because the specular reflection of parallel polarized radiation from a dielectric surface is very low at the Brewster angle which, for this sample, is near 60 deg.

The Brewster angle effect suggests that reflection from O.D. paint surfaces has a large component which can be attributed to specular reflection from a rough dielectric surface. This is even more clearly evident in the data plotted in Fig. 5. This plot is a cross plot of data from a number of θ_r scans such as those presented in Figs. 3 and 4. The fact that the cross polarized reflectances, $\rho'_{\perp,\parallel}$ and $\rho'_{\parallel,\perp}$, are nonzero suggests that there is an additional component to the bidirectional reflectance which is the result of multiple reflections on the surface and a penetration and scattering from within the paint medium which depolarizes the incident radiation.

The specular peak in Figs. 3 and 4 is fairly narrow. This suggests that the O.D. paint surface is, in fact, quite smooth. The small, fixed bistatic angle data in Fig. 6 most clearly indicate the degree of surface roughness. The bidirectional reflectance with 2β = 2 deg is very large at near normal incidence and falls off rapidly as the source and receiver are moved 10 deg away from the surface normal. Hence, it can be inferred that the surface is flat to within something like 10 deg.

The above general qualitative characteristics are common to all of the O.D. paint data, and they provide a firm foundation for the development of a bidirectional reflectance model for extrapolating a limited number of ρ' measurements at one wavelength to all source/receiver positions, polarizations, and wavelengths. The bidirectional reflectance model consists of two components. The first component takes into account the specular reflection from the rough dielectric surface which gives rise to most of the angular and polarization characteristics of the bidirectional reflectance. The second component is a volume component

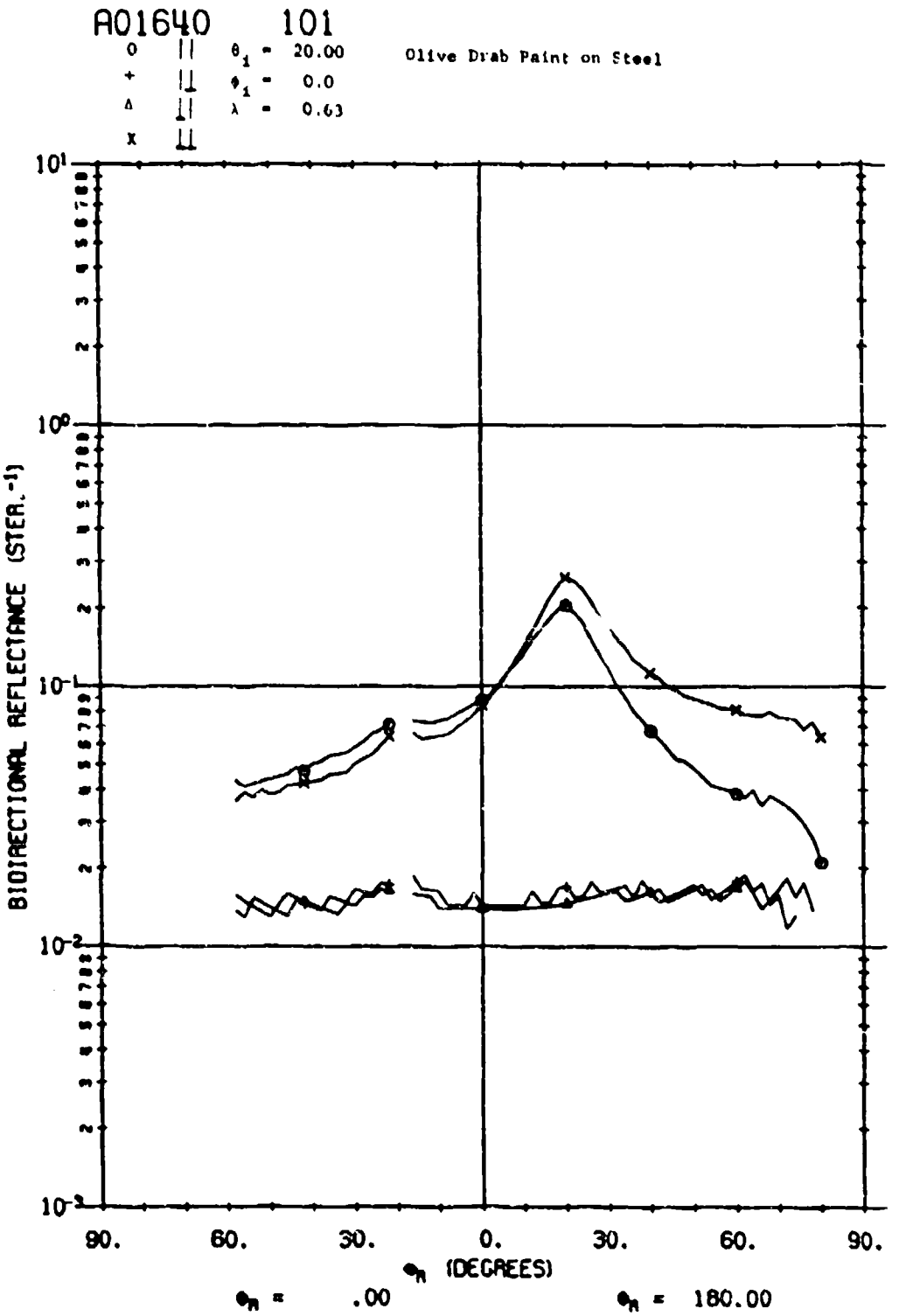

FIGURE 3. AN EXAMPLE OF ρ' FOR O.D. PAINT, $\theta_i = 20$

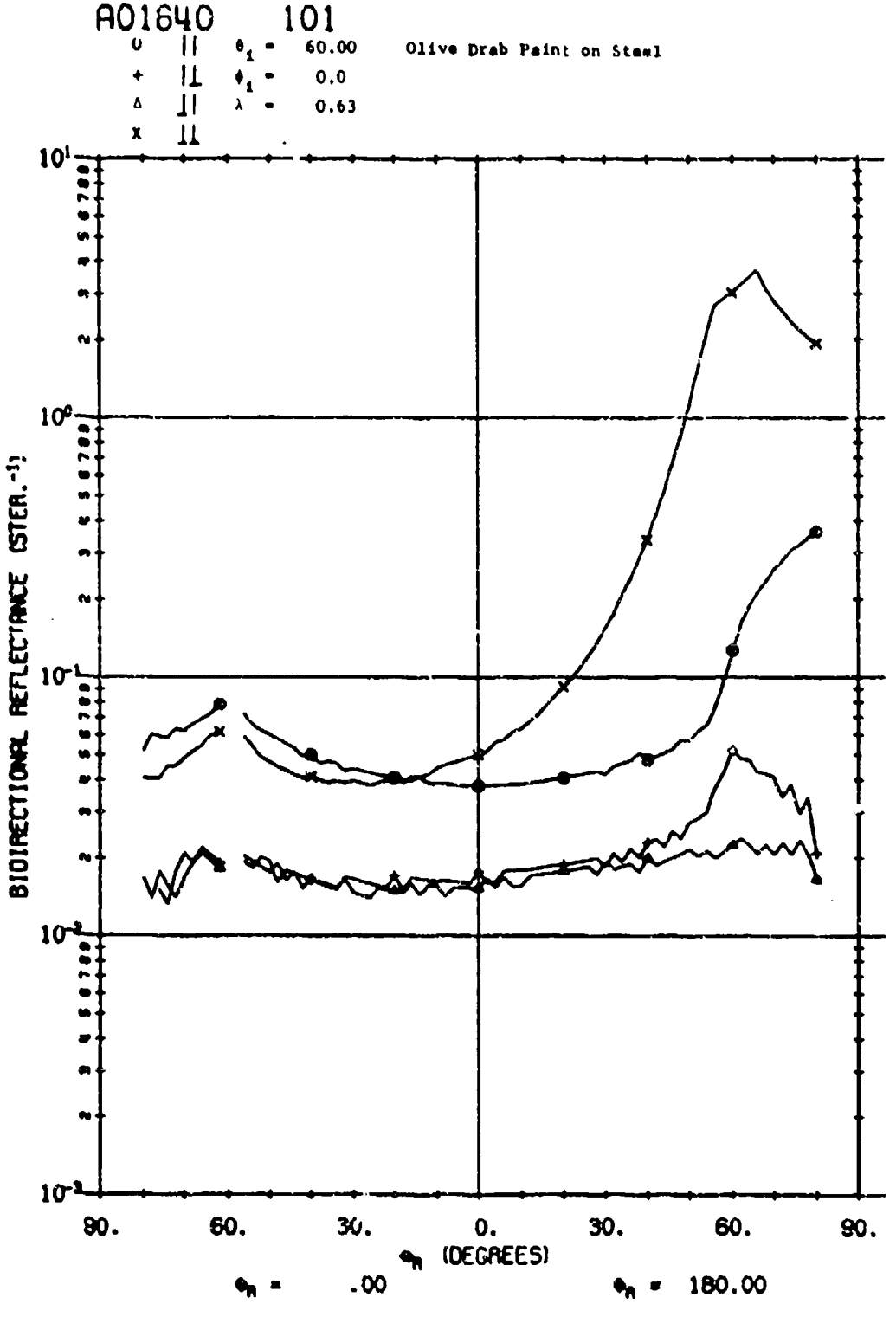

FIGURE 4. AN EXAMPLE OF ρ' FOR O.D. PAINT, $\theta_i = 60$

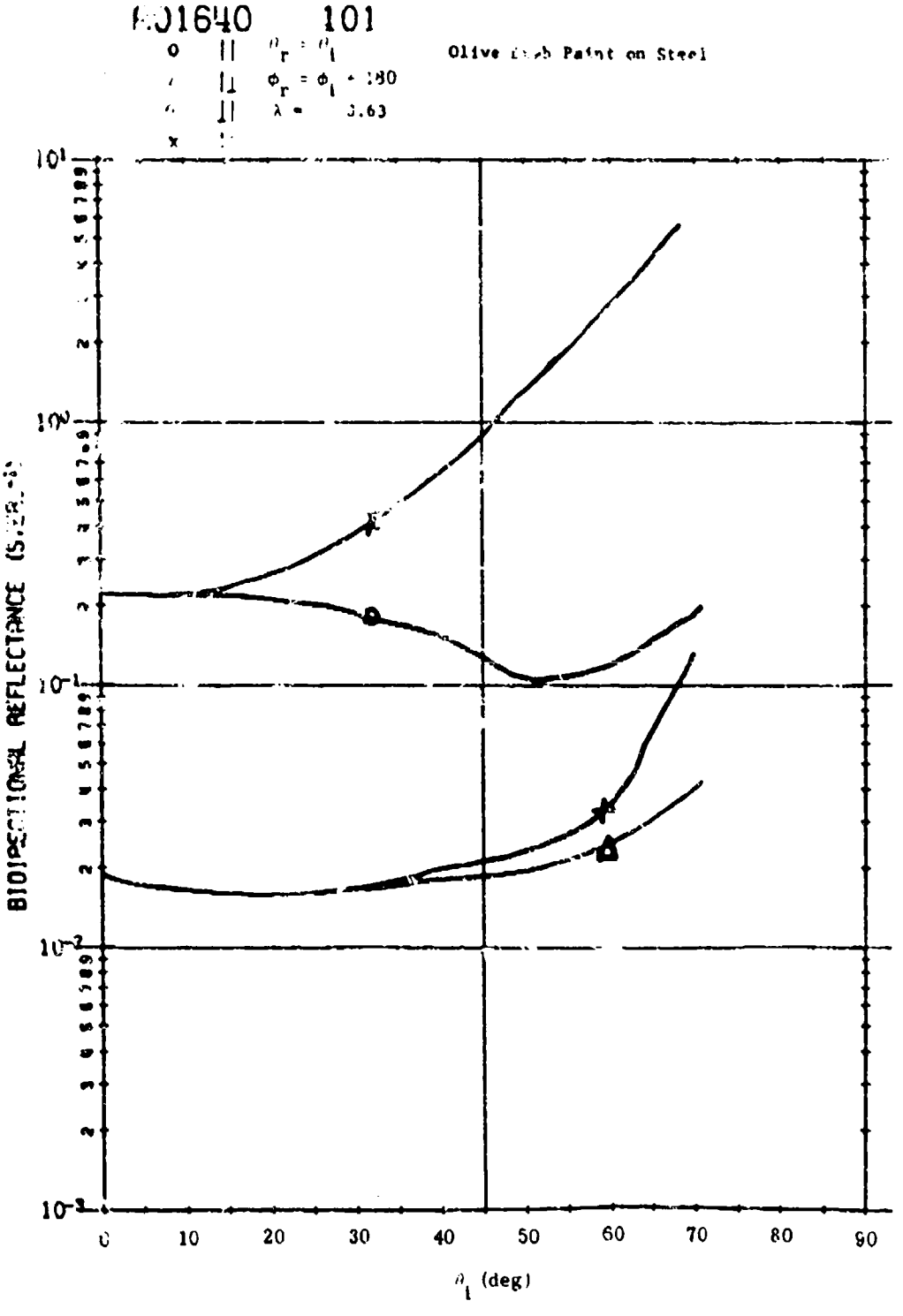

FIGURE 5. FRESNEL-LIKE BEHAVIOR OF ρ' (θ_i, 0;θ_i, 180) IN THE SPECULAR GEOMETRY

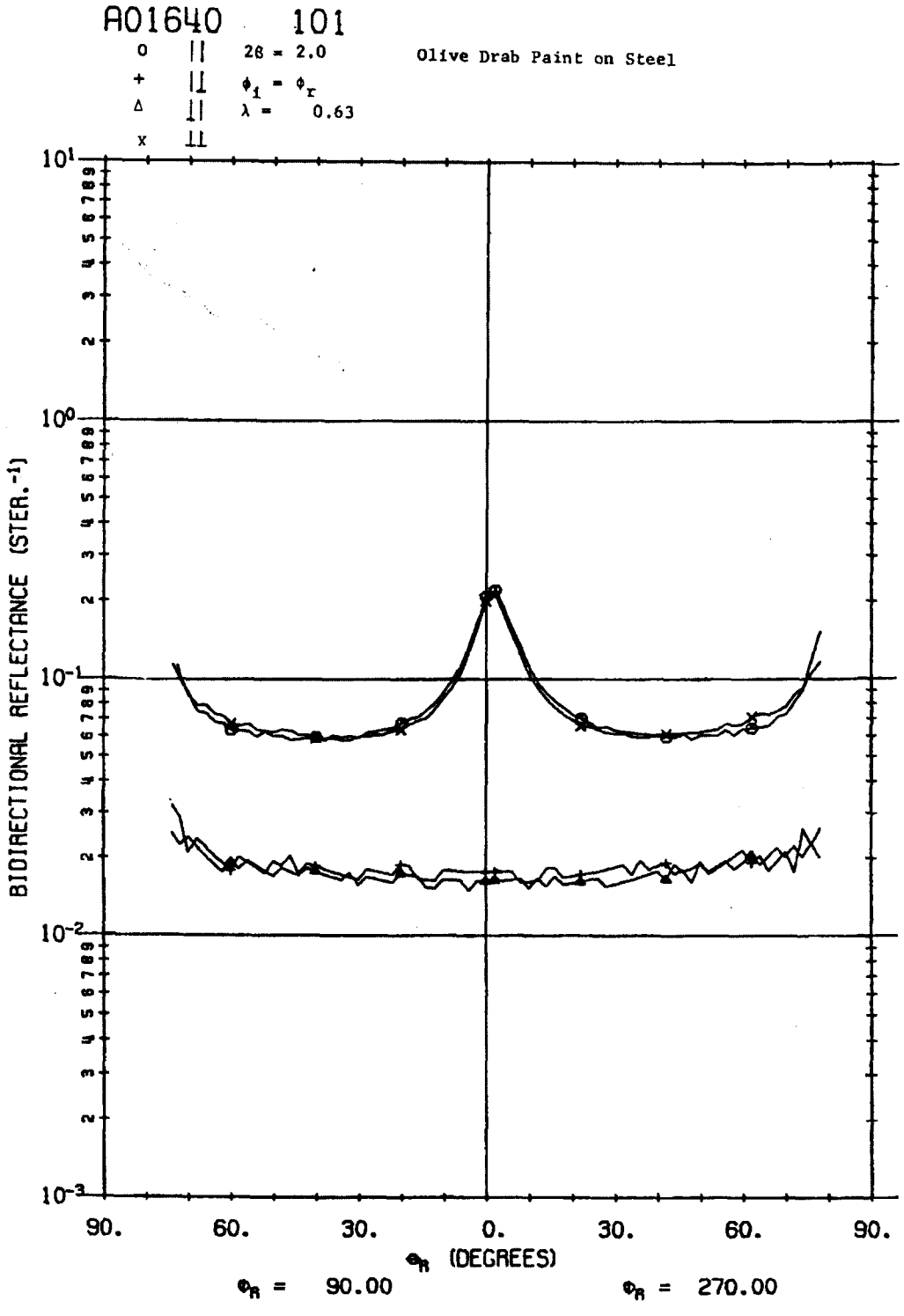

FIGURE 6. AN EXAMPLE OF ρ' FOR O.D. PAINT, $2\beta = 2$

which takes into account scattering and absorption from within the paint medium. This component gives rise to the more or less diffuse, unpolarized, and wavelength-dependent part of the bidirectional reflectance. The wavelength dependence of the volume component is obtained from the spectral directional-reflectance measurement data reported earlier in the Data Compilation.

4.2.2. SPECULARITY AT LONGER WAVELENGTHS

The reflectance properties of real surfaces are dependent both on the material's optical properties and surface properties. In the visible portion of the spectrum, almost all surfaces are rough compared to the wavelength (except those that are polished and which are mirror-like reflectors). In the microwave portion of the spectrum, most surfaces are smooth relative to the wavelength and are mirror-like reflectors. The characteristics of the bidirectional reflectance do not change very much from 0.63 to 1.06 μm, but there is a transition region where some surfaces are very smooth and others are still very rough and where the bidirectional reflectance changes character very dramatically. This transition occurs in the thermal infrared (IR) portion of the spectrum. The data exhibit this transition region in that the O.D. paint surfaces are very specular at 10.6 μm, whereas the various canvas, wood, and concrete and asphalt surfaces are nonspecular and still rough on a scale of 10.6 μm.

4.2.3. OTHER DATA CHARACTERISTICS

A characteristic common to many of the bidirectional reflectance curves in Volume II is that, over a rather large range of θ_r, (sometimes as large as 100 deg), the curves fall nearly on a curve described by some multiple of sec $(\theta_r - \theta_{r0})$; θ_{r0} is a constant which depends on θ_i and changes from one material to the next. The effect is most pronounced when the source is at a large angle of incidence. An example of this is shown in Fig. 7. This behavior is noticeably absent in the data known to satisfy Lambert's law fairly well, such as in the data for 3M-white paint (Fig. 8). This characteristic provides a guide for extrapolating the measured data to a wider range of $(\theta_i, \phi_i; \theta_r, \phi_r)$ and is a valuable key to the development of the volume component of the bidirectional reflectance model.

Another feature exhibited by the bidirectional reflectance data in Figs. 4 and 7, which has been found to be common to much of the ρ' data, is a pronounced increase in ρ' in the direct backscatter direction. This effect has been reported by Oetking [7] for a variety of materials.

4.2.4. REFLECTANCE STANDARDS DATA

A number of bidirectional reflectance measurements were made as a part of the laboratory phase of the Target Signature Measurements program to provide calibrated field reflectance standards for various other Air Force programs. Large canvas panels were used as reflectance standards for airborne measurement programs. Data were taken on these panels and are reported in the canvas and cloth data. Additional measurements were made on various materials in search of stable, reproducible, highly reflecting, and diffuse reflectors (ideally Labertian reflectors). The 3M-white paint, Fig. 8, was found to be the most nearly Lambertian

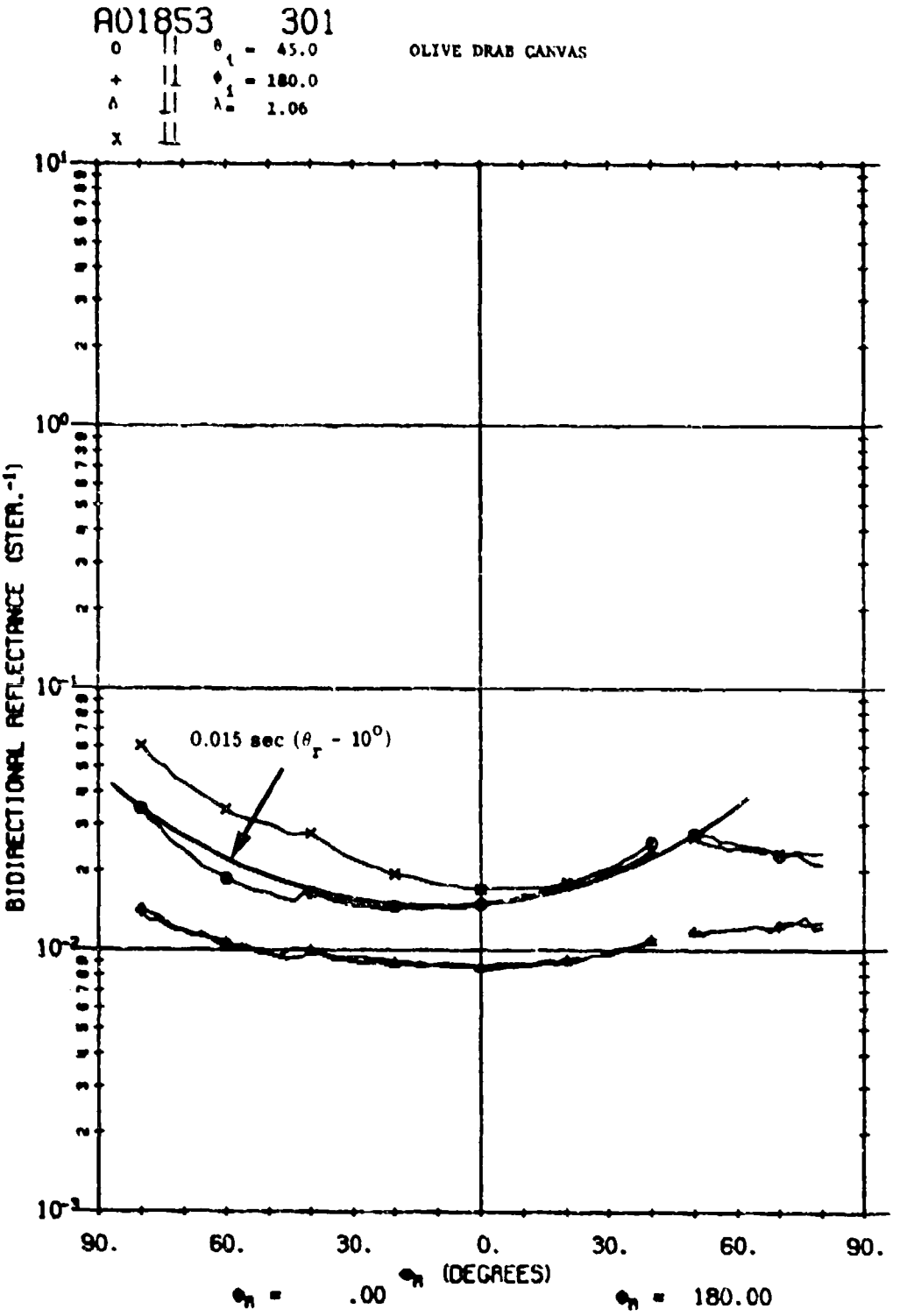

FIGURE 7. AN EXAMPLE OF THE sec (θ_r - θ_{ro}) DEPENDENCE OF ρ' FOR O.D. CANVAS

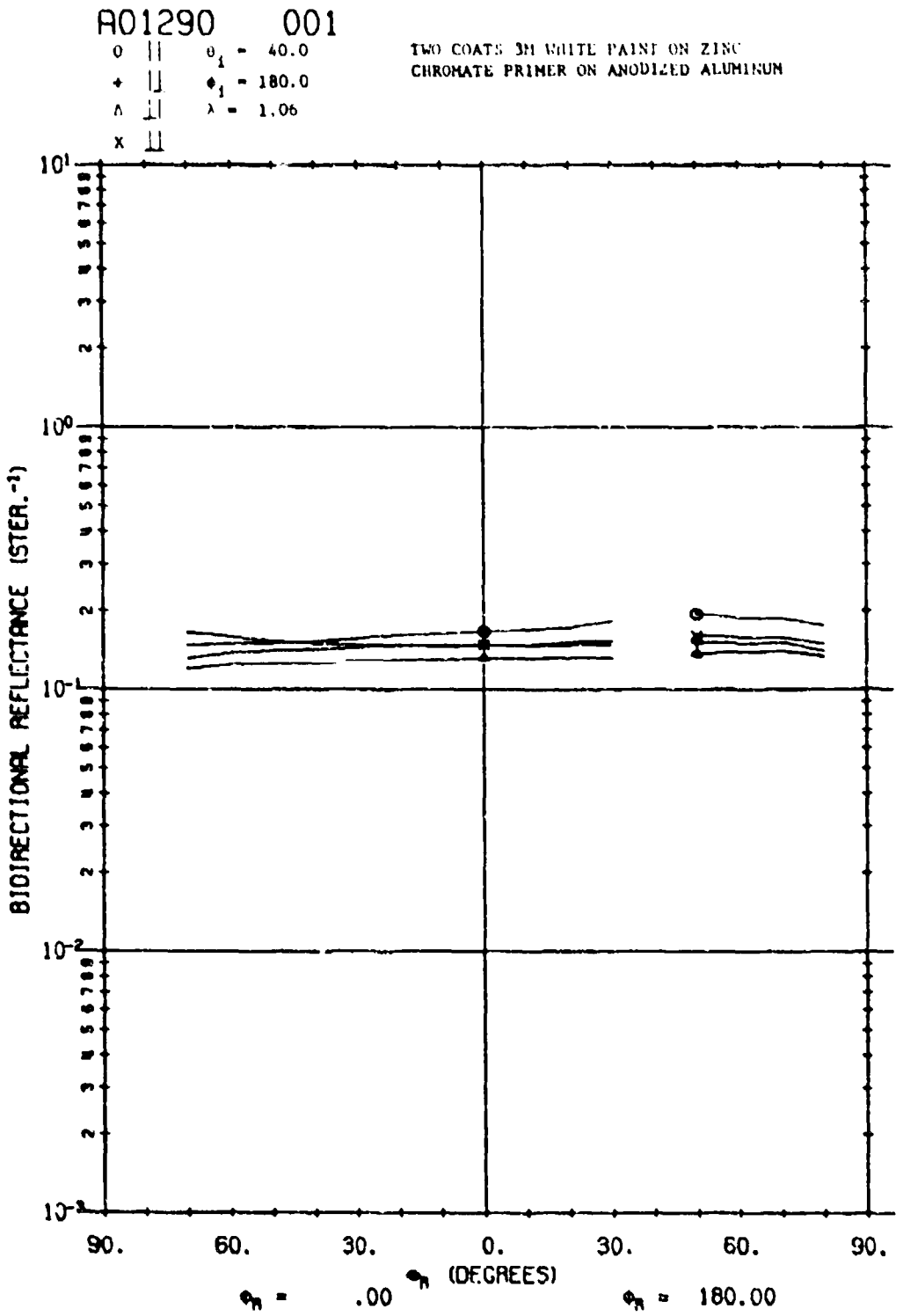

FIGURE 8. AN EXAMPLE OF ρ' FOR A 3M-WHITE REFERENCE STANDARD AT 0.63 μm

reflector and one of the most suitable diffuse field reflectance standards at 0.63 and 1.06 μm. Flame-sprayed aluminum, Fig. 9, was found to be nearly Lambertian and a good field reflectance standard in the infrared at 10.6 μm.

4.2.5. MEASUREMENT CHARACTERISTICS

The effects of the digital recording of the data and subsequent data processing are evident in some of the data. The bidirectional reflectance of a particular sample often varies by as much as three orders of magnitude, and this represents the limit of the dynamic range of the system. Usually, the high reflectance data are collected with attenuators in the system, and these are generally removed for collection of the low-reflectance data. For some measurements, the attenuators were not removed when the low reflectance data were collected. The effects of the digital processing are then apparent in these data because the bidirectional reflectance has to undergo a rather large fractional change to increment the digital voltmeter output. These data fall on segments of curves which are multiples of a sec θ_r curve, i.e., $n\Delta V \sec \theta_r$, where n is an integer and ΔV the smallest voltage increment of the digital voltmeter. The sec θ_r is the result of the $(\cos \theta_r)^{-1}$ factor in the data reduction formula, Eq. (5). A small ripple on the sec θ_r segments is caused by variation in the monitor voltage which is large compared to the signal voltage. Such data are illustrated with the $\rho'_{\parallel,\perp}$ and $\rho'_{\perp,\parallel}$ curves in Figs. 3, 4, and 6. The occurrence of segments of a sec θ_r curve resulting from the digital processing is an instrumentation effect and is not related to the sec $(\theta_r - \theta_{r0})$ effect observed in Section 4.2.3, a characteristic of the reflectance properties of many surfaces over some range of θ_r.

Several other characteristics appear in the data which are caused by the instrumentation. Data gaps appear in the backscatter direction when $\theta_r = \theta_i$, when the reveiver passes through the beam. No values of ρ' smaller than 10^{-3} inverse steradians are plotted, since this value of ρ' roughly represents the noise limit of the system. Finally, the earliest collected data (e.g. the data for paint sample A01295) were recorded on an analog strip chart recorder reduced manually at 5-deg angle increments. Straight lines connect the ρ' data points in these plots. Noise in these data is not evident as it is in the data collected later and recorded digitally at 1- or 2-deg incremets and computer processed.

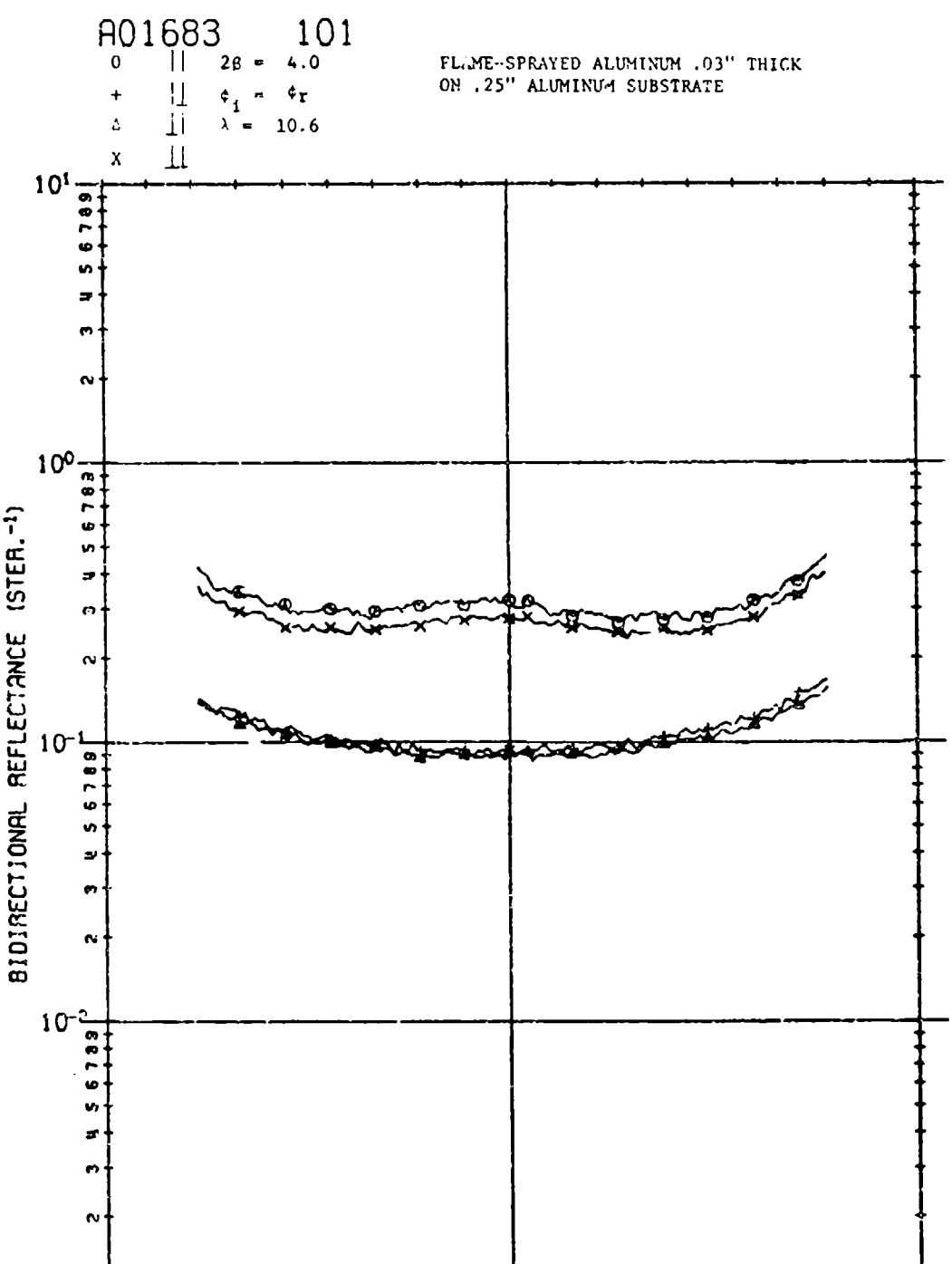

FIGURE 9. AN EXAMPLE OF ρ' FOR A FLAME-SPRAYED ALUMINUM REFERENCE STANDARD AT 10.6 μm

5
APPLICATIONS OF BIDIRECTIONAL REFLECTANCE DATA

Reflection characteristics of targets and backgrounds and appropriate associated equations are most often used to predict the operational capabilities of active or semiactive detection or mapping systems. When bidirectional reflectance data are used instead of the directional (an angle averaged) reflectance data, much better predictions can be made for the operation of such systems and errors caused by the assumption that a target is a diffuse reflector (when in actuality the reflector has nonuniform distribution properties) can be eliminated.

To obtain these better predictions, in addition the increased data-acquisition costs, it is necessary to work with large amounts of data since ρ' varies with both source and receiver directions. The manner in which ρ' varies depends on the particular surface considered and the polarization states of the source and receiver, as shown by the data curves in Volume II. For active detection or mapping systems in which the source and receiver are typically colinear, only the small, fixed, bistatic-angle data are needed. On the other hand, a full set of ρ' data is necessary for a passive system for which the sun illuminates the target and the location of which is completely independent of the location of the receiver.

The determination of relative contrasts likely to be evident in a strip map or other display can be made by ranking the angular dependent reflectance values for all targets and backgrounds that are to be included. An important assumption here is that ρ' data and geometric models are available for the targets and backgrounds considered.* A similar ranking of the directional reflectance values for the same targets and backgrounds is not an accurate way to predict relative contrasts because the angular reflection properties of materials vary so widely.

Another important advantage of using ρ' data lies in the polarization parameters that can be exploited to enhance contrast. Since the various polarized components usually have different values, there are many combinations --sums, differences, and ratios —than can be used with appropriate instrumentation to change the contrast between specified targets or target classes and their backgrounds. Much analysis is needed to determine the optimum source polarization plane or planes, receiver analyzer orientations, and/or signal processing. The result is potentially very significant because polarization effects are very pronounced in the data.

*The empirical models for extrapolating ρ' data obtained for a limited number of source-receiver positions and polarizations to all θ_i, ϕ_i, θ_r, ϕ_r, αi, αr, and a model to approximate a geometrically complex target surface as a collection of planar facets for reflection analysis have been developed by the Target Signature Analysis Center.

For a given system design, the received power for calculation of signal-to-noise ratio can be computed from the ρ' data. For flat surfaces, the ρ' data, as presented in Volume II, are appropriate. For geometrically complex targets, each flat elemental area on the target, with its appropriate $\rho'(\theta_i, \phi_i; \theta_r, \phi_r)$, has to be considered separately.

In the development which follows, no polarization subscripts are given to ρ'. The $\rho'_{\alpha i, \alpha r}$ appropriate to the polarization of the source and for the polarizer on the receiver is implied. Then, by definition (see Eq. 1):

$$\rho' = \frac{L^r(\theta_r, \phi_r)}{L^i(\theta_i, \phi_i) \cos \theta_i \, d\Omega_i} \tag{6}$$

where

$$L^i(\theta_i, \phi_i) \cos \theta_i \, d\Omega_i = E^i(\theta_i, \phi_i)$$

with $L^i(\theta_i, \phi_i)$ the radiance incident on the target from direction (θ_i, ϕ_i), and $d\Omega_i$ the incremental incidence solid angle about direction (θ_i, ϕ_i). Hence,

$$L^r(\theta_r, \phi_r) = \rho'(\theta_i, \phi_i; \theta_r, \phi_r) L^i(\theta_i, \phi_i) \cos \theta_i \, d\Omega_i \tag{7}$$

where a specified wavelength or narrow wavelength band is assumed. Then the radiant power P that passes through a remotely positioned aperture, $P(\theta_r, \phi_r)$, is

$$P(\theta_r, \phi_r) = L^r(\theta_r, \phi_r) A \cos \theta_r \Omega_r \tag{8}$$

where A = the area of the reflecting surface

Ω_r = the solid angle subtended by the receiving aperture

θ_r = the angle from the surface normal to the receiving aperture

It is assumed here that Ω_r is small and that the receiver is pointed directly toward the area A. Thus, generally

$$P(\theta_r, \phi_r) = \left[\int_{\Omega_i} \rho'(\theta_i, \phi_i; \theta_r, \phi_r) L^i(\theta_i, \phi_i) \cos \theta_i \, d\Omega_i \right] A \cos \theta_r \Omega_r \tag{9}$$

The term in the brackets is the target radiance $L^r(\theta_r, \phi_r)$ caused by the reflection of a source that subtends a solid angle Ω_i delivering radiance $L^i(\theta_i, \phi_i)$. This general equation can be simplified when certain conditions exist: if ρ' does not vary over the range of incidence angles considered, it can be moved outside the integral. The remaining integral is the irradiance E^i on the target. Under these conditions

$$P(\theta_r, \phi_r) = \rho'(\theta_i, \phi_i; \theta_r, \phi_r) E^i(\theta_i, \phi_i) A \cos \theta_r \Omega_r \tag{10}$$

With Eq. (10) as a starting point, substitutions can be made for the terms E, A, and Ω_r, in accordance with the geometries of various illumination source and receiver systems, to illustrate the use of ρ' data. Three equations are developed, one for solar illumination and two for laser illumination. It is assumed that only one target, for which ρ' is known, is in the field of view or is illuminated by the laser beam. An approximate answer for received power may be obtained if the target is assumed to be diffuse and ρ' is replaced by ρ_d/π (ρ_d being the directional reflectance reported earlier in the Data Compilation). However, this will lead to erroneous results if the target is specular and is the very reason for the use of ρ'.

Case I: Solar Illumination

The irradiance, E^i, from the sun is

$$E^i(\theta_i, \phi_i) = E_s \tau_a \cos \theta_i \tag{11}$$

where E_s is the solar constant, τ_a is the atmospheric transmission term for the selected wavelength band, and θ_i is the incidence angle.

If the receiver has a total angular field of view of α rad and is situated at an angle θ_r off the normal to the target surface, and if the range from receiver to target is R, then the target area A is

$$A = \frac{\pi}{4} R^2 \alpha^2 \frac{1}{\cos \theta_r} \tag{12}$$

The receiver solid angle Ω_r is simply receiver aperture area divided by the range from the source to the target

$$\Omega_r = \frac{A_{rec}}{R^2} \tag{13}$$

When these substitutions for E^i, A, and Ω_r are made into Eq. (10), for the case of solar illumination within a selected wavelength band, one obtains

$$P(\theta_r, \phi_r) = \rho'(\theta_i, \phi_i; \theta_r, \phi_r) E_s \tau_a \cos \theta_i \frac{\pi}{4} \alpha^2 A_{rec} \tag{14}$$

Equation (14) is independent of the range since, when the range to the receiver is decreased causing the solid angle to increase, the target area decreases. However, a term that is dependent on range, τ_{aR}, must be included to account for the atmospheric transmission between the target and the receiver. Thus, ignoring sky radiance incident on the target and any solar radiation scattered to the sensor by the intervening atmosphere, the complete equation for Case I is

$$P(\theta_r, \phi_r) = \rho'(\theta_i, \phi_i; \theta_r, \phi_r) E_s \tau_a \cos \theta_i \frac{\pi}{4} \alpha^2 A_{rec} \tau_{aR} \tag{15}$$

Case II: Laser Source Arranged Coaxially with a Receiver

The irradiance (on the target) caused by the laser source is

$$E^{l}(\theta_i, \phi_i) = \frac{P_t \cos \theta_i}{\frac{\pi}{4}\gamma^2 R^2} \tau_{at} \tag{16}$$

where P_t is the output power of the laser, γ is the beam divergence angle of the laser, and τ_{at} is the atmospheric transmission between the transmitter and the target; the remaining terms are as defined above. The target area and receiver solid angle are the same as in Case I; i.e.:

$$A = \frac{\pi}{4} R^2 \alpha^2 \frac{1}{\cos \theta_r}$$

Also

$$\Omega_r = \frac{A_{rec}}{R^2}$$

Upon substitution into Eq. (10), and ignoring the laser radiation scattered back to the receiver by the intervening atmosphere, the power at the receiver of a coaxially arranged laser illuminator, $P(\theta_r, \phi_r)$, at the receiver is

$$P(\theta_r, \phi_r) = \rho'(\theta, \phi; \theta, \phi) P_t \cos \theta \tau_{at}^2 \frac{\alpha^2}{\gamma^2} \frac{A_{rec}}{R^2} \tag{17}$$

where α^2/γ^2 is limited to 1.0, τ_{at} was squared to account for two-way propagation, and the subscript on θ was dropped since $\theta_r = \theta_i = \theta$ for a coaxial system. The term α^2/γ^2 in Eq. (17) has a maximum value of 1 since the portion of the field of view that is larger than the laser beamwidth does not contribute to received power.

Case III: Laser Source Not Arranged Coaxially with a Receiver

If the terms used to develop Eq. (17) are rewritten with subscripts to allow for a range R_t for the laser and R_R for the receiver

$$E^{l}(\theta_i, \phi_i) = \frac{P_t \cos \theta_i}{\frac{\pi}{4}\gamma^2 R_t^2} \tau_{at} \tag{18}$$

where τ_{at} is the atmospheric transmission from the laser source to the target

$$A = \frac{\pi}{4} R_R^2 \alpha^2 \frac{1}{\cos \theta_r}$$

and

$$\Omega_r = \frac{A_{rec}}{R_R^2}$$

Thus, with a laser and receiver not coaxial

$$P(\theta_r, \phi_r) = \rho'(\theta_i, \phi_i; \theta_r, \phi_r) P_t \cos \theta_i \tau_{at} \frac{\sigma^2}{\gamma^2} \cdot \frac{A_{rec}}{R_t^2} \tau_{aR} \tag{19}$$

where τ_{aR} is included as in Eq. (15).

The received power in Eqs. (15), (17), and (19) is directly proportional to the receiver aperture area. For certain types of targets, this is not true if large apertures are used. For example, if the target acts as a mirror in such a way that the beam properties of the source are conserved upon reflection, then the size of the receiver aperture relative to the reflected beam becomes important. For such a case, one would have to integrate ρ [illegible] the aperture area.

6
COMPLETE SPECIFICATION OF THE POLARIZED BIDIRECTIONAL REFLECTANCE

It is well known that four parameters are, in general, required to specify the polarization of the incident irradiance, $E^i(\theta_i, \phi_i)$, and that four are required to specify the polarization of the reflected radiance, $L^r(\theta_r, \phi_r)$, for incoherent radiation.* Hence, four measurements are required to completely determine the polarization state of a beam. The four parameters required to define an elliptically polarized beam are related to the intensity in the beam, its ellipticity, the orientation of the ellipse, and its handedness. These four parameters are conveniently contained in the four components of a four-element Stokes vector. The use of the Stokes vector to describe polarized radiation is well covered in Ref. [9]. The Stokes vector for polarized radiance $E^i(\theta_i, \phi_i)$ is denoted by $\left[E^i(\theta_i, \phi_i)\right]$, and similarly for the reflected radiance $L^r(\theta_r, \phi_r)$ by $\left[L^r(\theta_r, \phi_r)\right]$.

The transformation of the four component Stokes vector for the incident irradiance, $\left[E^i(\theta_i, \phi_i)\right]$, by the process of reflection to the four component Stokes vector for the reflected radiance, $\left[L^r(\theta_r, \phi_r)\right]$, involves a 4-by-4, 16-element Mueller matrix (Ref. 9). That is, a complete specification of the polarization characteristics of the bidirectional reflectance $\rho'(\theta_i, \phi_i; \theta_r, \phi_r)$ requires specification of 16 elements of a 4-by-4 matrix. The Mueller-matrix representation of the bidirectional reflectance is $[\rho'(\theta_i, \phi_i; \theta_r, \phi_r)]$. Then, in principle, 16 measurements with various combinations of source/receiver polarization have to be made of $\rho'(\theta_i, \phi_i; \theta_r, \phi_r)$ to determine the value of the 16 elements of $[\rho'(\theta_i, \phi_i; \theta_r, \phi_r)]$. In general, circularly polarized source polarizations are required to determine some of the elements and the circularly polarized components in the reflected radiance are required to determine some others. The number of elements needed in the $[\rho']$ matrix reduces to 12 when only plane polarized sources are considered. For surfaces which do not generate, upon reflection of plane polarized incident irradiance, a circularly polarized component in $L^r(\theta_r, \phi_r)$, the number of matrix elements needed is further reduced to 9. Then the number of polarized bidirectional reflectance measurements needed is also reduced to 12 and 9, respectively.

Only four combinations of source/receiver polarizations have been measured for most samples, namely, $\rho'_{\perp,\perp}$, $\rho'_{\perp,\parallel}$, $\rho'_{\parallel,\perp}$ and $\rho'_{\parallel,\parallel}$ and from these various others can be inferred which are appropriate to an unpolarized source and/or receiver (see Eq. 2). For a perpendicularly polarized source delivering $L^i_\perp(\theta_i, \phi_i)$ from direction (θ_i, ϕ_i) in a small solid angle $d\Omega_i$, the parallel and perpendicular components of the reflected radiance, $L^r_\parallel(\theta_r, \phi_r)$ and $L^r_\perp(\theta_r, \phi_r)$ are given by

*The laser produces coherent ratiation, but when the receiver subtends many speckles and when incoherent detection techniques are used, the use of Stokes vectors for incoherent radiation are still appropriate.

$$L^r_{\perp}(\theta_r, \phi_r) = \rho'_{\perp,\perp}(\theta_i, \phi_i; \theta_r, \phi_r) L^i_{\perp}(\theta_i, \phi_i) \cos\theta_i d\Omega_i$$

$$L^r_{\parallel}(\theta_r, \phi_r) = \rho'_{\perp,\parallel}(\theta_i, \phi_i; \theta_r, \phi_r) L^i_{\perp}(\theta_i, \phi_i) \cos\theta_i d\Omega_i$$

For a source which is distributed over a large solid angle Ω_i, but which is polarized $\perp$ to the plane of incidence everywhere in Ω_i

$$L^r_{\perp}(\theta_r, \phi_r) = \int_{\Omega_i} \rho'_{\perp,\perp}(\theta_i, \phi_i; \theta_r, \phi_r) L^i_{\perp}(\theta_i, \phi_i) \cos\theta_i d\Omega_i$$

$$L^r_{\parallel}(\theta_r, \phi_r) = \int_{\Omega_i} \rho'_{\perp,\parallel}(\theta_i, \phi_i; \theta_r, \phi_r) L^i_{\perp}(\theta_i, \phi_i) \cos\theta_i d\Omega_i$$

The equations for a source polarized parallel to the plane of incidence, and those with an unpolarized source take on a similar form.

It is very important to recognize that the bidirectional reflectance $\rho'_{\alpha i,\alpha r}$ for a linearly polarized source with αi other than 0(⊥) or 90(∥) cannot be determined from only $\rho'_{\perp,\perp}$, $\rho'_{\perp,\parallel}$, $\rho'_{\parallel,\perp}$ and $\rho'_{\parallel,\parallel}$ without additional ρ' measurements or a bidirectional reflectance model. These four polarized ρ' components are only 4 of the 12 (for plane polarized sources) required to specify $[\rho']$. Although a plane polarized incident radiance, $L_{\alpha i}(\theta_i, \phi_i)$, can be decomposed into components polarized parallel to the plane of incidence, $L^i_{\parallel}(\theta_i, \phi_i)$, and perpendicular to the plane of incidence, $L^i_{\perp}(\theta_i, \phi_i)$, vis.:

$$\begin{aligned} L^i_{\parallel}(\theta_i, \phi_i) &= L^i_{\alpha i}(\theta_i, \phi_i) \sin^2 \alpha i \\ L^i_{\perp}(\theta_i, \phi_i) &= L^i_{\alpha i}(\theta_i, \phi_i) \cos^2 \alpha i \end{aligned} \qquad (22)$$

so that

$$L^r_{\parallel}(\theta_r, \phi_r) = \rho'_{\parallel,\parallel}\left[L^i_{\alpha i}(\theta_i, \phi_i) \sin^2 \alpha i\right] \cos\theta_i d\Omega_i + \rho'_{\perp,\parallel}\left[L^i_{\alpha i}(\theta_i, \phi_i) \cos^2 \alpha i\right] \cos\theta_i d\Omega_i \qquad (23a)$$

and

$$L^r_{\perp}(\theta_r, \phi_r) = \rho'_{\parallel,\perp}\left[L^i_{\alpha i}(\theta_i, \phi_i) \sin^2 \alpha i\right] \cos\theta_i d\Omega_i + \rho'_{\perp,\perp}\left[L^i_{\alpha i}(\theta_i, \phi_i) \cos^2 \alpha i\right] \cos\theta_i d\Omega_i \qquad (23b)$$

the relative phase angle between the parallel and perpendicular polarized incident radiance changes upon reflection, so that we cannot determine $L^r_{\alpha r}(\theta_r, \phi_r)$ without additional ρ' measurements.

Fortunately, it is generally not necessary to make 16 (or even 12 or 9) measurements of ρ' with various source and receiver polarizations to determine all of the elements of the $[\rho']$ Mueller matrix. It is possible to infer all of them from only three of the four which have been measured, and which, for most samples, are reported with the empirical modeling techniques developed by the Target Signature Analysis Center. These same models also provide the complete $(\lambda;\ \theta_i,\phi_i;\ \theta_r,\phi_r)$ dependence from a very limited number of $\rho'(\lambda;\ \theta_i,\phi_i;\ \theta_r,\phi_r)$ measurements. The bidirectional reflectance models are thus very powerful tools indeed. Some of the modeling efforts have been applied to the complete reflection analysis of a geometrically complex target. Recent advances in the development of empirical bidirectional models by the Target Signature Analysis Center are soon to be published.

7
INDEX OF GRAPHIC BIDIRECTIONAL REFLECTANCE DATA IN VOLUME II AND CROSS REFERENCES

7.1 PAINTS

SAMPLE NO.	SAMPLE DESCRIPTION	λ	DATA PARAMETERS	PAGE
1027 003	OD Paint on Metal	0.63	θ_i = 0, 20, 40, 50, 60, 70; In-plane θ_r scan	1
1044 003	OD Paint on Metal	0.63	θ_i = 0, 20, 40, 50, 60, 70; In-plane θ_r scan	4
1047 003	OD Paint on Metal	0.63	θ_i = 0, 20, 40, 50, 60, 70; In-plane θ_r scan	7
1049 001	OD Paint on Metal	10.6	2s = 1.10; θ_r scan θ_i = 0, 50; In-plane θ_r scan	10
1187 001	Black Paint on Steel	0.63	θ_i = 0, 45, 70; In-plane θ_r scan	11
1224 004	OD Paint on Metal	0.63	θ_i = 0, 20, 30, 40, 60, 70; In-plane θ_r scan	13
1295 004	Lt. Green Paint on Metal	0.63	2s = 7; ϕ_r = 0, 180; θ_r scan 2s = 7; ϕ_r = 90, 270; θ_r scan θ_i = 0, 20, 30, 40, 60, 70; In-plane θ_r scan with ϕ_i = 90	16
1337 001	OD Paint on Metal	1.06	θ_i = 0, 60; In-plane θ_r scan	20
1338 001	OD Paint on Metal	1.06	θ_i = 0, 60; In-plane θ_r scan	21
1339 001	OD Paint on Metal	1.06	θ_i = 0, 60; In-plane θ_r scan	22
1341 006	OD Paint on Metal	0.63	2s = 7; ϕ_r = 0, 180; θ_r scan θ_i = 0, 20, 30, 40, 60, 70; In-plane θ_r scan 2s = 7, ϕ_r = 90, 270; θ_r scan	23
1342 005	OD Paint on Metal	0.63	2s = 7; ϕ_r = 0, 180; θ_r scan θ_i = 0, 20, 30, 40, 60, 70; In-plane θ_r scan 2s = 7; ϕ_r = 90, 270; θ_r scan	28
1343 004	OD Paint on Metal	0.63	2s = 7; ϕ_r = 0, 180; θ_r scan θ_i = 0, 20, 30, 40, 60, 70; In-plane θ_r scan 2s = 7; ϕ_r = 90, 270; θ_r scan	32

SAMPLE NO.	SAMPLE DESCRIPTION	λ	DATA PARAMETERS	PAGE
1444 004	Blue Paint on Metal	0.63	$2\theta = 7$; $\phi_r = 0, 180$; θ_r scan $\theta_i = 20, 30, 40, 60, 70$; In-plane θ_r scan $2\theta = 7$; $\phi_r = 90, 270$; θ_r scan	36
005		1.06	$2\theta = 7$; $\phi_r = 0, 180$; θ_r scan $\theta_i = 0, 20, 30, 40, 60, 70$; In-plane θ_r scan $2\theta = 7$; $\phi_r = 90, 270$; θ_r scan	39
1453 005	Lt. Brown Paint on Metal	0.63	$\theta_i = 0, 20, 30, 40, 60, 70$; In-plane θ_r scan with $\phi_i = 180$ $2\theta = 2$, $\phi_r = 90, 270$; θ_r scan	43
006		1.06	$2\theta = 7$; θ_r scan $\theta_i = 0, 20, 30, 40, 60, 70$; In-plane θ_r scan	47
1454 005	Field Drab Paint on Metal	0.63	$\theta_i = 0, 20, 30, 40, 60, 70$; In-plane θ_r scan with $\phi_i = 180$ $2\theta = 2$; $\phi_r = 90, 270$; θ_r scan	51
004	Field Drab Paint on Metal	1.06	$2\theta = 7$; θ_r scan $\theta_i = 0, 20, 30, 40, 60, 70$; In-plane θ_r scan	54
1455 005	OD Paint on Metal	0.63	$2\theta = 2$; θ_r scan $\theta_i = 0, 30, 70$; In-plane θ_r scan	57
1456 005	OD Paint on Metal	0.63	$2\theta = 2$; $\phi_r = 0, 180$; θ_r scan $\theta_i = 0, 20, 30, 40, 60, 70$; In-plane θ_r scan $2\theta = 2$; $\phi_r = 90, 270$; θ_r scan	59
004		1.06	$2\theta = 7$; θ_r scan $\theta_i = 0, 20, 30, 40, 60, 70$; In-plane θ_r scan	63
1457 006	OD Paint on Metal	0.63	$2\theta = 2$; $\phi_r = 0, 180$; θ_r scan $\theta_i = 0, 30, 70$; In-plane θ_r scan with $\phi_i = 0$ $2\theta = 2$; $\phi_r = 0, 180$; θ_r scan	67

SAMPLE NO.	SAMPLE DESCRIPTION	λ	DATA PARAMETERS	PAGE
1457 006	OD Paint on Metal	0.63	θ_i = 0, 30, 70; In-plane θ_r scan with ϕ_i = 180 2B = 2; ϕ_r = 90, 270; θ_r scan θ_i = 0, 30, 70; In-plane θ_r scan with ϕ_i = 270	67
005		1.06	2B = 7; ϕ_r = 0, 180; θ_r scan θ_i = 0, 20, 30, 40, 60, 70; In-plane θ_r scan with ϕ_i = 0 θ_i = 20, 30, 40, 60, 70; In-plane θ_r scan with ϕ_i = 180 2B = 7; ϕ_r = 90, 270; θ_r scan θ_i = 0, 20, 30, 40, 60, 70; In-plane θ_r scan with ϕ_i = 270	73
1509 001	OD Paint on Metal	0.63	θ_i = 0, 45; In-plane θ_r scan	82
1569 003	Green Paint on Steel	0.63	2B = 2; θ_r scan θ_i = 0, 30, 70; In-plane θ_r scan	83
004		10.6	2B = 1; θ_r scan θ_i = 0, 20, 30, 40, 60, 70, In-plane θ_r scan	86
1570 004	Lt. Brown Paint on Metal	0.63	2B = 2; θ_r scan θ_i = 0, 30, 70; In-plane θ_r scan	89
003		10.6	2B = 1.1; θ_i scan θ_i = 0, 20, 30, 40, 60, 70; In-plane θ_r scan	91
1586 001	Blue Metallic Paint on Steel	10.6	2B = 1.1; θ_r scan θ_i = 0, 50; In-plane θ_r scan	95
1567 001	Green Metallic Paint on Steel	10.6	2B = 1.1; θ_r scan θ_i = 0, 50; In-plane θ_r scan	96
1588 001	Red Paint on Steel	10.6	2B = 1.1; θ_r scan θ_i = 0, 50; In-plane θ_r scan	98
1569 001	White Paint on Plywood	10.6	2B = 1.1; ϕ_r = 0, 180; θ_r scan 2B = 1.1; ϕ_r = 90, 270; θ_r scan	99

SAMPLE NO.	SAMPLE DESCRIPTION	λ	DATA PARAMETERS	PAGE
1608 201	OD Paint on Metal	0.63	θ_i = 0, 10, 20, 30, 40, 45, 50, 55, 60, 65, 70, 75, 80; In-plane θ_r scan	100
1610 101	OD Paint on Metal	10.6	θ_i = 0, 10, 20, 30, 40, 50; In-plane θ_r scan	107
1629 101	OD Paint on Metal	0.63	θ_i = 0, 10, 20, 30, 35, 40, 45, 50, 55, 60, 70; In-plane θ_r scan	109
1638 101	Light Tan Paint on Metal	0.63	θ_i = 0, 40, 70; In-plane θ_r scan	115
1640 101	OD Paint on Metal	0.63	θ_i = 0, 10, 20, 30, 40, 50, 60, 70; In-plane θ_r scan with ϕ_i = 180 2β = 2; ϕ_r = 90, 270; θ_r scan	116
1699 301	Black Paint on Metal	0.63	θ_i = 0, 30, 60; In-plane θ_r scan	121
302		1.06	θ_i = 0; In-plane θ_r scan	
1701 102	OD Paint on Metal	0.63	2β = 2; θ_r scan θ_i = 0, 30, 60, 80; In-plane θ_r scan θ_i = 0, 30, 60; Out-of-plane θ_r scan θ_i = 45; ϕ_r scan	123
201		0.63	2β = 2; θ_r scan θ_i = 30, 60; In-plane θ_r scan θ_i = 0, 30, 60; Out-of-plane θ_r scan	127
101		10.6	2β = 1; θ_r scan θ_i = 0, 30, 60; In-plane θ_r scan θ_i = 0, 30, 60; Out-of-plane θ_r scan	130
1807 301	Camouflage Paint on Metal	0.63	2β = 2; ϕ_r = 0, 180; θ_r scan θ_i = 0, 10, 20, 30, 40, 50, 60, 70; In-plane θ_r scan with ϕ_i = 180	143
301	Camouflage Paint on Metal	0.63	2β = 2; ϕ_r = 90, 270; θ_r scan θ_i = 0, 10, 20, 30, 40, 50, 60, 70; In-plane θ_r scan with ϕ_i = 270	143

SAMPLE NO.	SAMPLE DESCRIPTION	λ	DATA PARAMETERS	PAGE
1807 101		1.06	$2\beta = 2$; θ_r scan $\theta_i = 0, 10, 20, 30, 40, 50, 60, 70, 75$; In-plane θ_r scan $\theta_i = 10, 20, 30, 40, 50, 60, 70$; Out-of-plane θ_r scan	152
302		10.6	$\theta_i = 0, 10$; In-plane θ_r scan	161
1808 301	Camouflage Paint on Metal	0.63	$\theta_i = 0$; In-plane θ_r scan	162
101		1.06	$2\beta = 2$; θ_r scan $\theta_i = 0$; In-plane θ_r scan	162
1839 301	OD Paint on Metal	1.06	$2\beta = 2$; θ_r scan $\theta_i = 0$; In-plane θ_r scan	163
1848 301	OD and White Paint on Metal	1.06	$\theta_i = 0, 30, 45, 60, 75$; In-plane θ_r scan with $\phi_i = 180$ $2\beta = 2, 5, 10$; $\phi_r = 90, 270$; θ_r scan	164
1879 201	Green Paint on Metal	10.6	$2\beta = 2$; $\phi_r = 0, 180$; θ_r scan $\theta_i = 0$; In-plane θ_r scan $2\beta = 2$; $\phi_r = 90, 270$; θ_r scan	168
1880 201	Green Paint on Metal	10.6	$2\beta = 2$; $\phi_r = 0, 180$; θ_r scan $\theta_i = 0$; In-plane θ_r scan $2\beta = 2$; $\phi_r = 90, 270$; θ_r scan $\theta_i = 0$; In-plane θ_r scan	170
1881 301	Black Paint on Metal	10.6	$2\beta = 2$; $\phi_r = 0, 180$; θ_r scan $\theta_i = 0$; In-plane θ_r scan $2\beta = 2$; $\phi_r = 90, 270$; θ_r scan $\theta_i = 0$; In-plane θ_r scan	172
1882 201	Orange Paint on Metal	10.6	$2\beta = 2$; $\phi_r = 0, 180$; θ_r scan $\theta_i = 0$; In-plane θ_r scan $2\beta = 2$; $\phi_r = 90, 270$; θ_r scan	174
1883 101	OD Paint on Metal	10.6	$2\beta = 2$; $\phi_r = 0, 180$; θ_r scan $\theta_i = 0$; In-plane θ_r scan $2\beta = 2$; $\phi_r = 90, 270$; θ_r scan	175
1887 201	Blue Paint on Metal	10.6	$2\beta = 2$; $\phi_r = 0, 180$; θ_r scan $\theta_i = 0$; In-plane θ_r scan $2\beta = 2$; $\phi_r = 90, 270$; θ_r scan	177

SAMPLE NO.	SAMPLE DESCRIPTION	λ	DATA PARAMETERS	PAGE
1888 201	OD Paint on Metal	10.6	$2\beta = 2$; $\phi_r = 0, 180$; θ_r scan $\theta_i = 0$; In-plane θ_r scan $2\beta = 2$; $\phi_r = 90, 270$; θ_r scan $\theta_i = 0$; In-plane θ_r scan	178
1889 101	OD Paint on Metal	10.6	$2\beta = 2$; θ_r scan $\theta_i = 0$; In-plane θ_r scan	180
1892 301	OD Paint on Metal	10.6	$2\beta = 2$; θ_r scan $\theta_i = 0$; In-plane θ_r scan	181
1897 101	3M Black Paint on Wood	10.6	$2\beta = 2$; θ_r scan $\theta_i = 0, 40$; In-plane θ_r scan	182
1917 101	OD Paint on Metal	10.6	$2\beta = 2$; θ_r scan $\theta_i = 0$; In-plane θ_r scan	184
1920 101	OD Paint on Cork	10.6	$2\beta = 2$; θ_r scan $\theta_i = 0$; In-plane θ_r scan	185
1922 101	OD Paint on Posterboard	10.6	$2\beta = 2$; θ_r scan $\theta_i = 0$; In-plane θ_r scan	186
1924 101	OD Paint on Plexiglass	10.6	$2\beta = 2$; θ_r scan $\theta_i = 0$; In-plane θ_r scan	187
1926 101	OD Paint on Cardboard	10.6	$2\beta = 2$; θ_r scan $\theta_i = 0$; In-plane θ_r scan	188
2001 101	OD Paint on Metal	1.06	$2\beta = 2$; θ_r scan $\theta_i = 0, 56$; In-plane θ_r scan $\theta_i = 56$; Out-of-plane θ_r scan	189
2004 101	OD Paint on Metal	1.06	$2\beta = 2$; θ_r scan $\theta_i = 0, 56$; In-plane θ_r scan $\theta_i = 56$; Out-of-plane θ_r scan	191

CROSS REFERENCES FOR PAINT

1290 0C1 3M White Paint (See Reflectance Standards Material)
1292 001 " " " " " " "

1460 401	3M White Paint (See Reflectance Standards Material)
1466 002	Black Paint on Canvas (See Cloth and Canvas)
1470 101	Medium Gray Paint on Canvas (See Cloth and Canvas)
1471 002	" " " " " " " " "
1474 002	Grayish-White Paint on Canvas (See Cloth and Canvas)
1475 101	" " " " " " " " "
1478 002	Green Paint on Canvas (See Cloth and Canvas)
2003 101	3M White Paint on Fiberboard (See Reflectance Standards Material)

7.2 CLOTH AND CANVAS

SAMPLE NO.	SAMPLE DESCRIPTION	λ	DATA PARAMETERS	PAGE
1013 007	Blue Gray Cotton	0.63	θ_i = 0, 40; In-plane θ_r scan with ϕ_i = 180 θ_i = 0, 40; In-plane θ_r scan with ϕ_i = 270	193
1057 014	White Nylon	0.63	θ_i = 30; In-plane θ_r scan	195
1058 014	Olive Green Nylon	0.63	θ_i = 30; In-plane θ_r scan	195
1059 014	Orange Nylon	0.63	θ_i = 30; In-plane θ_r scan	196
1059 015	Orange Nylon	0.63	θ_i = 30; In-plane θ_r scan	196
1060 014	Sand (Beige) Nylon	0.63	θ_i = 30; In-plane θ_r scan	197
1061 014	Olive Green Nylon	0.63	θ_i = 30; In-plane θ_r scan	197
1096 002	Green Canvas	10.6	2θ = 1.1; θ_r scan θ_i = 0, 50; In-plane θ_r scan	198
1099 002	White Canvas	10.6	2θ = 1.1; θ_r scan θ_i = 0, 50; In-plane θ_r scan	199
1103 002	Black Canvas	10.6	2θ = 1.1; θ_r scan θ_i = 0, 50; In-plane θ_r scan	201
1188 007	Faded Black Cotton	0.63	θ_i = 0, 40; In-plane θ_r scan with ϕ_i = 180 θ_i = 0, 40; In-plane θ_r scan with ϕ_i = 270	202
1189 008	Gray-Green Cotton Drill	0.63	θ_i = 0, 40; In-plane θ_r scan with ϕ_i = 180 θ_i = 0, 40; In-plane θ_r scan with ϕ_i = 270	204

SAMPLE NO.	SAMPLE DESCRIPTION	λ	DATA PARAMETERS	PAGE
1466 002	Black Paint on Canvas	10.6	$2\beta = 1.1$; θ_r scan $\theta_i = 0, 50$; In-plane θ_r scan	206
1470 101	Gray Paint on Canvas	0.63	$\theta_i = 0, 10, 20, 30, 40, 50, 60, 70$; In-plane θ_r scan	208
002		10.6	$2\beta = 1.1$; θ_r scan $\theta_i = 0, 50$; In-plane θ_r scan	212
1471 002	Gray Paint on Canvas	10.6	$2\beta = 1.1$; θ_r scan $\theta_i = 0, 50$; In-plane θ_r scan	212
1474 002	Grayish-White Paint on Canvas	10.6	$2\beta = 1.1$; θ_r scan $\theta_i = 0, 50$; In-plane θ_r scan	215
1475 101	Grayish-White Paint on Canvas	0.63	$\theta_i = 0, 10, 20, 30, 40, 50, 60, 70$; In-plane θ_r scan	216
1478 002	Green Paint on Canvas	10.6	$2\beta = 1.1$; θ_r scan $\theta_i = 0, 50$; In-plane θ_r scan	220
1480 002	Undyed Cotton	10.6	$2\beta = 1.1$; θ_r scan $\theta_i = 0, 50$; In-plane θ_r scan	222
1483 002	Vat Dyed Cotton	10.6	$2\beta = 1.1$; θ_r scan $\theta_i = 0, 50$; In-plane θ_r scan	223
1486 002	Cotton, Sulfer Dye	10.6	$2\beta = 1.1$; θ_r scan $\theta_i = 0, 50$; In-plane θ_r scan	225
1510 001	OD Canvas Tarpaulin	0.63	$\theta_i = 0, 45$; In-plane θ_r scan	226
1667 101	Red Canvas	0.63	$\theta_i = 0, 20, 40, 60$; In-plane θ_r scan	227
103		0.63	$\theta_i = 0, 20, 40, 60$; In-plane θ_r scan	229
102		1.15	$\theta_i = 0, 20, 40, 60$; In-plane θ_r scan	231
1668 102	Blue Canvas	0.46	$\theta_i = 0, 20, 40, 60$; In-plane θ_r scan	233
101		0.63	$\theta_i = 0, 20, 40, 60$; In-plane θ_r scan	235

SAMPLE NO.	SAMPLE DESCRIPTION	λ	DATA PARAMETERS	PAGE
1668 104		0.63	θ_i = 0, 20, 40, 60; In-plane θ_r scan	237
103	Blue Canvas	1.15	θ_i = 0, 20, 40, 60; In-plane θ_r scan	239
1669 101	Green Canvas	0.63	θ_i = 0, 20, 40, 60; In-plane θ_r scan	241
104		0.63	θ_i = 0, 20, 40, 60; In-plane θ_r scan	243
103		1.15	θ_i = 0, 20, 40, 60; In-plane θ_r scan	245
1670 102	Gray Treated Canvas	0.46	θ_i = 0, 20, 40, 60; In-plane θ_r scan	247
101		0.63	θ_i = 0, 20, 40, 60; In-plane θ_r scan	249
1671 102	Gray Treated Canvas	0.46	θ_i = 0, 20, 40, 60; In-plane θ_r scan	251
101	Gray Treated Canvas	0.63	θ_i = 0, 20, 40, 60; In-plane θ_r scan	253
1672 102	Gray Treated Canvas	0.46	θ_i = 0, 20, 40, 60; In-plane θ_r scan	255
101		0.63	θ_i = 0, 20, 40, 60; In-plane θ_r scan	257
1673 103	Gray Treated Canvas	0.46	θ_i = 0, 20, 40, 60; In-plane θ_r scan	259
101		0.63	θ_i = 0, 20, 40, 60; In-plane θ_r scan	261
102		0.63	θ_i = 0, 20, 40, 60; In-plane θ_r scan	263
1674 101	Black Treated Canvas	0.63	θ_i = 0, 20, 40, 60; In-plane θ_r scan	265
102		0.63	θ_i = 0, 20, 40, 60; In-plane θ_r scan	267

SAMPLE NO.	SAMPLE DESCRIPTION	λ	DATA PARAMETERS	PAGE
1680 101	OD Canvas	0.63	θ_i = 0, 20, 40, 60; In-plane θ_r scan	269
301		10.6	2θ = 2; θ_r scan θ_i = 0; In-plane θ_r scan	271
1802 101	Gray Canvas	0.63	θ_i = 0, 20, 40, 60, 75; In-plane θ_r scan with ϕ_i = 90 θ_i = 0, 20, 40, 60, 75; Out-of-plane θ_r scan with ϕ_i = 0	272
1803 101	Black Canvas	0.63	θ_i = 0, 20, 40, 60,65; In-plane θ_r scan with ϕ_i = 90 θ_i = 0, 20, 40, 60, 75; Out-of-plane θ_r scan with ϕ_i = 0	273
1820 101	Gray Canvas	10.6	2θ = 2; θ_r scan θ_i = 0, 40; In-plane θ_r scan	274
1853 301	OD Canvas	1.06	θ_i = 0,30,45; In-plane θ_r scan with ϕ_i = 180 2θ = 2; ϕ_r = 90,270; θ_r scan θ_i = 60,75; In-plane θ_r scan with ϕ_i = 180	
1890 101	OD Canvas	10.6	2θ = 2; θ_r = 0, 180; θ_r scan θ_i = 0; In-plane θ_r scan 2θ = 2; θ_r = 90, 270; θ_r scan	287
1891 101	Vinyl Coated OD Canvas	10.6	2θ = 2; θ_r scan θ_i = 0; In-plane θ_r scan	288
1893 101	OD Canvas	10.6	2θ = 2; θ_r scan θ_i = 0; In-plane θ_r scan	289
1900 101	Vinyl Coated OD Canvas	10.6	2θ = 2; θ_r scan θ_i = 0; In-plane θ_r scan	290
1918 101	Black Canvas	1.06	θ_i = 0, 56; In-plane θ_r scan θ_i = 56; Out-of-plane θ_r scan	291
1919 201	Black Canvas	1.06	2θ = 2; θ_r scan θ_i = 56; In-plane θ_r scan	293
2002 101	OD Canvas	1.06	θ_i = 0, 56; In-plane θ_r scan θ_i = 56; Out-of-plane θ_r scan	294

7.3 WOOD

SAMPLE NO.	SAMPLE DESCRIPTION	λ	DATA PARAMETERS	PAGE
0096 004	Redwood Block	10.6	2θ = 1.1; ϕ_r = 0, 180; θ_r scan θ_i = 0, 50; In-plane θ_r scan 2θ = 1.1; ϕ_r = 90, 270; θ_r scan θ_i = 0, 50; In-plane θ_r scan	297
0106 002	White Oak Block	10.6	2θ = 1.1; ϕ_r = 0, 180; θ_r scan θ_i = 0, 50; In-plane θ_r scan 2θ = 1.1; ϕ_r = 90, 270; θ_r scan θ_i = 0, 50; In-plane θ_r scan	300
0118 002	Red Oak Block	10.6	2θ = 1.1; ϕ_r = 0, 180; θ_r scan θ_i = 0, 50; In-plane θ_r scan 2θ = 1.1; ϕ_r = 90, 270; θ_r scan θ_i = 0, 50; In-plane θ_r scan	303
0137 002	California White Oak Block	10.6	2θ = 1.1; ϕ_r = 0, 180; θ_r scan θ_i = 0, 50; In-plane θ_r scan 2θ = 1.1; ϕ_r = 90, 270; θ_r scan θ_i = 0; In-plane θ_r scan	306
0153 002	White Pine Block	10.6	2θ = 1.1; ϕ_r = 0, 180; θ_r scan θ_i = 0, 50; In-plane θ_r scan 2θ = 1.1; ϕ_r = 90, 270; θ_r scan θ_i = 0, 50; In-plane θ_r scan	308
0167 002	Oregon White Oak Block	10.6	2θ = 1.1; ϕ_r = 0, 180; θ_r scan θ_i = 0, 50; In-plane θ_r scan 2θ = 1.1; ϕ_r = 90, 270; θ_r scan θ_i = 0, 50; In-plane θ_r scan	311
1585 001	Untreated Wood	10.6	2θ = 1.1; ϕ_r = 0, 180; θ_r scan θ_i = 0, 50; In-plane θ_r scan 2θ = 1.1; ϕ_r = 90, 270; θ_r scan θ_i = 0, 50; In-plane θ_r scan	314
1590 001	Unpainted Plywood	10.6	2θ = 1.1; ϕ_r = 0, 180; θ_r scan 2θ = 1.1; ϕ_r = 90, 270; θ_r scan	317

SAMPLE NO.	SAMPLE DESCRIPTION	λ	DATA PARAMETERS	PAGE
1699 101	Wood	0.63	$2\theta = 2$; $\phi_r = 0, 180$; θ_r scan $\theta_i = 0, 30, 60, 65, 80$; In-plane θ_r scan with $\phi_i = 180$ $\theta_i = 0, 30, 60$; Out-of-plane θ_r scan with $\phi_i = 180$ $\theta_i = 0, 30, 60$; In-plane θ_r scan with $\phi_i = 270$ $\theta_i = 45$; ϕ_r scan	318
102		1.06	$2\theta = 2$; ϕ_r scan $\theta_i = 0, 30, 60$; In-plane θ_r scan with $\phi_i = 180$ $\theta_i = 0, 30, 60$; Out-of-plane θ_r scan with $\phi_i = 180$ $\theta_i = 45$; ϕ_r scan	325

CROSS REFERENCES FOR WOOD

1585 001 Creosote Treated Wood (See Miscellaneous)

1589 001 White Paint on Plywood (See Paint)

7.4 SOIL

SAMPLE NO.	SAMPLE DESCRIPTION	λ	DATA PARAMETERS	PAGE
1959 101	Sand	10.6	$2\theta = 2.5$, θ_r scan	329
**9010 014	Red Clay, Dry	.4920	$\theta_i = 53$; In-plane θ_r scan	329
019		.5200	$\theta_i = 45$; In-plane θ_r scan	330
C17			$\theta_i = 80$; In-plane θ_r scan	330
006		.6430	$\theta_i = 0$; In-plane θ_r scan	331
005			$\theta_i = 23$; In-plane θ_r scan	331
004			$\theta_i = 37$; In-plane θ_r scan	332
003			$\theta_i = 53$; In-plane θ_r scan	332
002			$\theta_i = 66$; In-plane θ_r scan	333
001			$\theta_i = 78$; In-plane θ_r scan	333
020	Red Clay, Wet	.5200	$\theta_i = 45$; In-plane θ_r scan	334
018			$\theta_i = 80$; In-plane θ_r scan	334
041	White Quarts Sand	.4920	$\theta_i = 53$; In-plane θ_r scan	335
030		.6430	$\theta_i = 0$; In-plane θ_r scan	335
029			$\theta_i = 23$; In-plane θ_r scan	336

SAMPLE NO.	SAMPLE DESCRIPTION	λ	DATA PARAMETERS	PAGE
9010 028	White Quartz Sand	.6430	θ_i = 37; In-plane θ_r scan	336
027			θ_i = 53; In-plane θ_r scan	337
026			θ_i = 66; In-plane θ_r scan	337
025			θ_i = 78; In-plane θ_r scan	338
039		.7060	θ_i = 53; In-plane θ_r scan	338
045	White Gypsum Sand	.5200	θ_i = 60; In-plane θ_r scan	339
046	Black Loam Soil	.5200	θ_i = 60; In-plane θ_r scan	339

**The data with Sample Numbers 9010 were taken from Reference [5]

7.5 VEGETATION

SAMPLE NO.	SAMPLE DESCRIPTION	λ	DATA PARAMETERS	PAGE
1324 001	Mature Mulberry Leaf	0.63	θ_i = 0, 20, 40, 50, 60, 70; In-plane θ_r scan	341
1327 001	Merion Blue Grass	0.63	θ_i = 0, 20, 40, 50, 60, 70; In-plane θ_r scan	344
1516 003	Tree Bark	10.6	2β = 1.1; θ_r scan θ_i = 0, 50; In-plane θ_r scan	347
1517 002	Pine Tree Bark	10.6	2β = 1.1; θ_r scan θ_i = 0, 50; In-plane θ_r scan	348

7.6 ASPHALT AND CONCRETE

SAMPLE NO.	SAMPLE DESCRIPTION	λ	DATA PARAMETERS	PAGE
1329 001	Concrete	0.63	θ_i = 0, 20, 40, 50, 60, 70; In-plane θ_r scan	351
1530 002	Fine Textured Concrete	10.6	2β = 1.1; ϕ_r = 0, 180; θ_r scan θ_i = 0, 50; In-plane θ_r scan 2β = 1.1; ϕ_r = 90, 270; θ_r scan θ_i = 0, 50; In-plane θ_r scan	354
1537 002	Very Fine Concrete	10.6	2β = 1.1; ϕ_r = 0, 180; θ_r scan θ_i = 0, 50; In-plane θ_r scan 2β = 1.1; ϕ_r = 90, 270; θ_r scan θ_i = 0, 50; In-plane θ_r scan	357

SAMPLE NO.	SAMPLE DESCRIPTION	λ	DATA PARAMETERS	PAGE
1543 002	Medium Fine Asphalt	10.6	$2\beta = 1.1$; $\phi_r = 0, 180$; θ_r scan $\theta_i = 0, 50$; In-plane θ_r scan $2\beta = 1.1$; $\phi_r = 90, 270$; θ_r scan $\theta_i = 0, 50$; In-plane θ_r scan	360
1546 002	Medium Fine Asphalt	10.6	$2\beta = 1.1$; $\phi_r = 0, 180$; θ_r scan $\theta_i = 0, 50$; In-plane θ_r scan $2\beta = 1.1$; $\phi_r = 90, 270$; θ_r scan $\theta_i = 50$; In-plane θ_r scan	363

7.7 REFLECTANCE STANDARDS MATERIAL

SAMPLE NO.	SAMPLE DESCRIPTION	λ	DATA PARAMETERS	PAGE
1094 001	Flame Sprayed Aluminum	10.6	$2\beta = 1.1$; θ_r scan $\theta_i = 0, 50$; In-plane θ_r scan	367
1095 001	Flame Sprayed Copper	10.6	$2\beta = 1.1$; θ_r scan $\theta_i = 0, 50$; In-plane θ_r scan	368
1190 001	Smoked Magnesium Oxide	0.63	$\theta_i = 0, 20, 40, 60$; In-plane θ_r scan	370
1191 001	Fiberfrax Type 970 JH	0.43	$\theta_i = 0, 80$; In-plane θ_r scan	372
		0.55	$\theta_i = 80$; In-plane θ_r scan	
		0.75	$\theta_i = 80$; In-plane θ_r scan	
		1.10	$\theta_i = 80$; In-plane θ_r scan	
002		0.55	$\theta_i = 0$; In-plane θ_r scan	
		0.63	$\theta_i = 0, 40$; In-plane θ_r scan	374
		0.75	$\theta_i = 0$; In-plane θ_r scan	
		1.10	$\theta_i = 0$; In-plane θ_r scan $\theta_i = 0$; Out-of-plane θ_r scan	
1192 001	Flowers of Sulfer	0.63	$\theta_i = 0$; In-plane θ_r scan	377
1194 001	Chrome Plated Glass Beads	0.63	$\theta_i = 0, 40$; In-plane θ_r scan	378
1197 001	Sandblasted Aluminum	0.54	$\theta_i = 10$; In-plane θ_r scan	379
002		1.08	$\theta_i = 10$; In-plane θ_r scan	379
1272 001	Chrome Plated Glass Beads	1.06	$\theta_i = 0, 30, 60, 80$; In-plane θ_r scan	380

SAMPLE NO.	SAMPLE DESCRIPTION	λ	DATA PARAMETERS	PAGE
1290 001	3M White Paint	1.06	θ_i = 0, 20, 30, 40, 60, 70; In-plane θ_r scan	382
1292 001	3M White Paint	1.06	θ_i = 0; In-plane θ_r scan	385
002			θ_i = 0; In-plane θ_r scan	385
003			θ_i = 0, 60; In-plane θ_r scan	386
1293 001	Fiberfrax Type 970 JH	1.06	θ_i = 0, 20, 30, 40, 50, 60, 70; In-plane θ_r scan	387
1296 001	Sandblasted Copper Plated Stainless Steel	1.06	θ_i = 0, 20, 30, 40, 60, 70; In-plane θ_r scan	390
101		10.6	2β = 2; θ_r scan θ_i = 0, 40; In-plane θ_r scan	393
1297 101	White Salt Standard	10.6	2β = 2; θ_r scan θ_i = 0, 40; In-plane θ_r scan	395
1317 001	Pressed Magnesium Oxide	0.63	θ_i = 0, 40; In-plane θ_r scan	396
1331 101	Gold Plated Silicon Carbide Paper	10.6	2β = 2; θ_r scan θ_i = 0, 40; In-plane θ_r scan	397
1332 001	Copper Plated Stainless Steel	1.06	θ_i = 0, 20, 30, 40, 60, 70; In-plane θ_r scan	399
1435 101	Electro-Plated Copper	10.6	2β = 2; θ_r scan θ_i = 0, 40; In-plane θ_r scan	402
1460 401	3M White Paint	0.63	θ_i = 0; In-plane θ_r scan	403
1598 101	Gold Plated, Sandblasted Stainless Steel	10.6	2β = 2; θ_r scan θ_i = 0, 40; In-plane θ_r scan	404
1683 102	Flame-Sprayed Aluminum	0.63	2β = 2; ϕ_r = 0, 180; θ_r scan θ_i = 0, 30, 50, 70; In-plane θ_r scan 2β = 2; ϕ_r = 90, 270; θ_r scan θ_i = 30, 50, 70; Out-of-plane θ_r scan	405
101		10.6	2β = 4; θ_r scan	410

SAMPLE NO.	SAMPLE DESCRIPTION	λ	DATA PARAMETERS	PAGE
1684 101	Flame-Sprayed Aluminum	10.6	$2\theta = 2$; θ_r scan $\theta_i = 0, 40$; In-plane θ_r scan	410
1688 101	Flame-Sprayed Aluminum	10.6	$2\theta = 2$; θ_r scan $\theta_i = 0, 40$; In-plane θ_r scan	412
1894 101	Flame-Sprayed Aluminum	10.6	$2\theta = 2$; θ_r scan $\theta_i = 0$; In-plane θ_r scan	413
1895 101	Sandblasted Aluminum	10.6	$2\theta = 2$; θ_r scan $\theta_i = 0$; In-plane θ_r scan	414
201			$2\theta = 2$; θ_r scan $\theta_i = 0$; In-plane θ_r scan	415
301			$2\theta = 2$; θ_r scan $\theta_i = 0$; In-plane θ_r scan	416
1896 101	Sandblasted Galvanized Steel	10.6	$2\theta = 2$; θ_r scan $\theta_i = 0$; In-plane θ_r scan	417
201			$2\theta = 2$; θ_r scan $\theta_i = 0$; In-plane θ_r scan	418
1915 101	Flame-Sprayed Aluminum	10.6	$2\theta = 2$; θ_r scan $\theta_i = 0$; In-plane θ_r scan	419
1916 101	Flame-Sprayed Aluminum	10.6	$2\theta = 2$; θ_r scan $\theta_i = 0$; In-plane θ_r scan	420
2003 101	3M White Paint on Fiberboard	1.06	$\theta_i = 0, 56$; In-plane θ_r scan $\theta_i = 56$; Out-of-plane θ_r scan	421

CROSS REFERENCES FOR REFLECTANCE STANDARDS MATERIAL

1466 002 Black Paint on Canvas, 4% Reflectance (See Cloth and Canvas)

1470 101 Gray Paint on Canvas, 16% Reflectance (See Cloth and Canvas)

002 " " " " " " " " " "

1471 002 Gray Paint on Canvas, 16% Reflectance (See Cloth and Canvas)

1474 002 Grayish-White Paint on Canvas, 64% Reflectance (See Cloth and Canvas)

1475 101 " " " " " " " " " " "

1670 102 Gray Treated Canvas, 64% Reflectance (See Cloth and Canvas)

101 " " " " " " " " "

CROSS REFERENCES FOR REFLECTANCE STANDARDS MATERIAL (Continued)

1671 102 Gray Treated Canvas, 32% Reflectance (See Cloth and Canvas)

101 " " " " " " " " "

1672 102 Gray Treated Canvas, 16% Reflectance (See Cloth and Canvas)

101 " " " " " " " " "

1673 103 Gray Treated Canvas, 8% Reflectance (See Cloth and Canvas)

101 " " " " " " " " "

102 " " " " " " " " "

1674 101 Black Treated Canvas, 4% Reflectance (See Cloth and Canvas)

102 " " " " " " " " "

1802 101 Gray Canvas, 8% Reflectance (See Cloth and Canvas)

1803 101 Black Canvas, 4% Reflectance (See Cloth and Canvas)

7.8 METAL

SAMPLE NO.	SAMPLE DESCRIPTION	λ	DATA PARAMETERS	PAGE
1294 004	Bare Metal	0.63	$2\theta = 7$; θ_r scan $\theta_i = 0, 20, 30, 40, 60, 70$; In-plane θ_r scan	423
1336 001	Alclad Aluminum Panel	1.06	$\theta_i = 0, 60$; In-plane θ_r scan	427
1699 201	Bare Metal	0.63	$\theta_i = 0, 30, 60$; In-plane θ_r scan $\theta_i = 0, 30, 60$; Out-of-plane θ_r scan $\theta_i = 45$; ϕ_r scan	428
1884 201	Galvanized Pipe	10.6	$2\theta = 2$; $\phi_r = 0, 180$; θ_r scan $\theta_i = 0$; In-plane θ_r scan $2\theta = 2$; $\phi_r = 90, 270$; θ_r scan $\theta_i = 0$; In-plane θ_r scan	431
1885 201	Galvanized Pipe	10.6	$2\theta = 2$; $\phi_r = 0, 180$; θ_r scan $\theta_i = 0$; In-plane θ_r scan $2\theta = 2$; $\phi_r = 90, 270$; $\theta_i = 0$; In-plane θ_r scan	433
1886 201	Galvanized Pipe	10.6	$2\theta = 2$; $\phi_r = 0, 180$; θ_r scan $\theta_i = 0$; In-plane θ_r scan $2\theta = 2$; $\phi_r = 90, 270$; θ_r scan $\theta_i = 0$; In-plane θ_r scan	435

CROSS REFERENCES FOR METAL

1094 001	Flame Sprayed Aluminum (See Reflectance Standards Material)
1095 001	Flame Sprayed Copper (See Reflectance Standards Material)
1194 001	Chrome Plated Glass Beads (See Reflectance Standards Material)
1272 001	" " " " " " " "
1296 001	Sandblasted Copper Plated Aluminum (See Reflectance Standards Material)
1331 101	Gold Plated Silicon Carbide Paper (See " " ")
1332 001	Copper Plated Stainless Steel(See Reflectance Standards Material)
1337 001	OD Paint on Metal (See Paint)
1338 001	OD Paint on Metal (See Paint)
1683 102	Flame-Sprayed Aluminum (See Reflectance Standards Material)
1684 101	" " " " " " "
1688 101	" " " " " " "
1820 101	C . Canvas Treated with a Metallic Coating (See Cloth and Canvas)
1894 101	. e Sprayed Aluminum (See Reflectance Standards Material)
1895 101	Sandblasted Aluminum (See " " ")
1896 101	Sandblasted Galvanized Steel (See Reflectance Standards Material)
1915 101	Flame Sprayed Aluminum (See Reflectance Standards Material)
1916 101	" " " " " " "

7.9 MISCELLANEOUS

SAMPLE NO.	SAMPLE DESCRIPTION	λ	DATA PARAMETERS	PAGE
1584 001	Creosote Treated Wood	10.6	$2\beta = 1.1$; $\phi_r = 0, 180$; θ_r scan $\theta_i = 0, 50$; In-plane θ_r scan $2\beta = 1.1$; $\phi_r = 90, 270$; θ_r scan $\theta_i = 0, 50$; In-plane θ_r angle	439
1921 101	Pressed Cork	10.6	$2\beta = 2$; θ_r scan $\theta_i = 0$; In-plane θ_r scan	442
1923 101	White Posterboard	10.6	$2\beta = 2$; θ_r scan $\theta_i = 0$; In-plane θ_r scan	443
1925 101	Acrylic Plexiglass	10.6	$2\beta = 2$; θ_r scan $\theta_i = 0$, In-plane θ_r scan	444
1927 101	Brown Corrugated Cardboard	10.6	$2\beta = 2$; θ_r scan $\theta_i = 0$; In-plane θ_r scan	445

DISTRIBUTION LIST

Air Force Avionics Laboratory
Wright-Patterson Air Force Base, Ohio 45433
ATTN: AFAL/RSP/Mr. Grimberg (1)

Air Force Avionics Laboratory
Wright-Patterson Air Force Base Ohio 45433
ATTN: AFAL RSA Avionics Central (1)

Air Force Avionics Laboratory
Wright-Patterson Air Force Base, Ohio 45433
ATTN: AFAL/RSP Mr. Richard Jennewine (1)

Air Force Avionics Laboratory
Wright-Patterson Air Force Base, Ohio 45433
ATTN: AFAL/RSP, Mr. Bruno K. Wernicke (1)

Air Force Avionics Laboratory
Wright-Patterson Air Force Base, Ohio 45433
ATTN: AFAL/AAM/Capt Fred Howard (1)

Air Force Avionics Laboratory
Wright-Patterson Air Force Base, Ohio 45433
ATTN: AFAL/RSE/Mr. W. C. Caulfield (1)

Air Force Avionics Laboratory
Wright-Patterson Air Force Base, Ohio 45433
ATTN: AFAL/NVN-1/Lt Lester McFawn (1)

Air Force Avionics Laboratory
Wright-Patterson Air Force Base, Ohio 45433
ATTN: AFAL/NVT/Mr. Robert L. Mawdsley (1)

Air Force Avionics Laboratory
Wright-Patterson Air Force Base, Ohio 45433
ATTN: AFAL/NVT/(LASE)/Mr. Donald Stevison (1)

Air Force Avionics Laboratory
Wright-Patterson Air Force Base, Ohio 45433
ATTN: AFAL/RSE/Mr. J. W. Crouch (1)

Aeronautical Systems Division
Wright-Patterson Air Force Base, Ohio 45433
ATTN: ASD ENVWA-40/Mr. H. L. Williams (1)

Aeronautical Systems Division
Wright-Patterson Air Force Base, Ohio 45433
ATTN: ASD ENRS/ Mr. Lee W. Cunningham (1)

Aeronautical Systems Division
Wright-Patterson Air Force Base, Ohio 45433
ATTN: ASD INH (1)

Rome Air Development Center
Griffiss Air Force Base, New York 13442
ATTN: INAP/Mr. Ragazzo (1)

Rome Air Development Center
Griffiss Air Force Base, New York 13442
ATTN: RADC/INR/Data Base (1)

Air Force Armament Laboratory
Eglin Air Force Base, Florida 32542
ATTN: ATTT/Mr. Long (1)

6585 Test Group
Holloman Air Force Base, New Mexico 88330
ATTN: GD/Dr. Martin Jaenicke (1)

Air Force Weapons Laboratory
Kirtland Air Force Base, New Mexico 87117
ATTN: WLIL (1)

Air University Library
Maxwell Air Force Base, Alabama 36112 (1)

ADTC (TSGPA)
Eglin Air Force Base, Florida 32542
ATTN: Mr. Franklin Gay (1)

USAFTAWC (AYN)
Eglin Air Force Base, Florida 32542
ATTN: Maj Robert L. Ingram (1)

Headquarters SAC (INEP)
Offutt Air Force Base, Nebraska 68113 (1)

Space and Missile Systems Organization
Los Angeles Air Force Station, California 90045
ATTN: SYAS (1)

Air Force Materials Laboratory
Wright-Patterson Air Force Base, Ohio 45433
ATTN: AFML/LAM Mr. J. H. Charlesworth (1)

Air Force Materials Laboratory
Wright-Patterson Air Force Base, Ohio 45433
ATTN: AFML/LPT/Mr. R. M. Van Vliet (1)

Headquarters, ESD (YW) Stop-15
L. G. Hanscom Field
Bedford, Massachusetts 01730 (1)

The RAND Corporation
1700 Main Street
Santa Monica, California 90406
ATTN: Library - D (1)

Air Force Cambridge Research Laboratories
L. G. Hanscom Field
Bedford, Massachusetts 01730
ATTN: AFCRL/LWH/ Dr. John F. Cronin (1)

Air Force Cambridge Research Laboratories
L. G. Hanscom Field
Bedford, Massachusetts 01730
ATTN: OPA/Dr. Robert Fenn (1)

Air Force Cambridge Research Laboratories
L. G. Hanscom Field
Bedford, Massachusetts 01730
ATTN: AFCRL/PHL/Dr. Salisbury (1)

Air Force Cambridge Research Laboratories
L. G. Hanscom Field
Bedford, Massachusetts 01730
ATTN: LZ/Mr. C. J. Sletten (1)

Headquarters, USAF
Washington, D.C. 20330
ATTN: RDPJ (1)

Headquarters, USAF
Washington, D.C. 20330
ATTN: SAMID (1)

AFSC Liaison Office
Langley Research Center (NASA)
Langley Air Force Base, Virginia 23365 (1)

Technical Library
Building 305
Aberdeen Proving Ground, Maryland 21005
ATTN: LWL/ Mr. H. Forst (1)

Director, Human Engineering Laboratory
Aberdeen Proving Ground, Maryland 21005
ATTN: Mr. John D. Weisz (1)

Commanding Officer
Coating and Chemical Laboratory
Aberdeen Proving Ground, Maryland 21005
ATTN: RD-CS/Dr. James McLeskey (1)

Commanding Officer
U.S. Army Mobility Equipment Research and Development Center
Fort Belvoir, Virginia 22060
ATTN: Technical Document Center, SMEFB-MW/Mr. D. Gee (1)

Commanding Officer
U.S. Army Mobility Equipment Research and Development Center
Fort Belvoir, Virginia 22060
ATTN: SMEFB-MW (Countersurveillance Branch) (1)

Commanding Officer
U.S. Army Frankford Arsenal
Philadelphia, Pennsylvania 19137

ATTN: SMUFA-N5100 Mr. Jacob H. Kubanoff (1)

U.S. Army Behavior and System Research Laboratory
1300 Wilson Boulevard
The Rosslyn Commonwealth Building
Arlington, Virginia 22209

ATTN: CRDMRC/BESRL D (1)

Commanding Officer
U.S. Army Topographical Command
6500 Brooks Lane
Washington, D.C. 20315

ATTN: PIRD (85000), Dr. J. N. Rinker (1)

Commanding General
U.S. Army Missile Command
Advanced Sensors Laboratory
Redstone Arsenal, Alabama 35809

ATTN: AMSMI-RER/Mr. L. W. Root (1)

Commanding General
U.S. Army Missile Command
Advanced Sensors Laboratory
Redstone Arsenal, Alabama 35809

ATTN: Physical Sciences Directorate/Dr. Herbert Holl (1)

Commanding Officer
U.S. Army Natick Laboratories
Natick, Massachusetts 01760

ATTN: AMXRE-CTR/Mr. Frank Rizzo (1)

Director
U.S. Army Engineer Waterways Experiment Station
Vicksburg, Mississippi 39180

ATTN: WESFT (1)

Commanding General
U.S. Army Research and Development Center
Ballistic Research Laboratory
Aberdeen Proving Ground, Maryland 21005

ATTN: AMXBR-BSP/Dr. D. Reuyl (1)

Commanding General
U.S. Army Research and Development Center
Ballistic Research Laboratory
Aberdeen Proving Ground, Maryland 21005

ATTN: AMXBR/Mr. A. Downs (1)

Commanding General
U.S. Army Research and Development Center
Ballistic Research Laboratory
Aberdeen Proving Ground, Maryland 21005

ATTN: AMXBR-BSP/Mr. D. Menne (1)

Commanding General
U.S. Army Research and Development Center
Ballistic Research Laboratory
Aberdeen Proving Ground, Maryland 21005

ATTN: AMXRD/BSP/Mr. James Rapp (1)

U.S. Army Electronics Command
Night Vision Laboratory
Fort Belvoir, Virginia 22060

ATTN: AMSEL-NV-VI Dr. M. L. Vatsia (1)

Commanding General
U.S. Army Electronics Command
Fort Monmouth, New Jersey 07703

ATTN: AMSEL-CT-HDR (1)

Commanding General
U.S. Army Electronics Command
Fort Monmouth, New Jersey 07703

ATTN: AMSEL-CT-L Mr. Bluford (1)

Commanding General
U.S.Army Electronics Command
Fort Monmouth, New Jersey 07703

ATTN: AMSEL-HL-CT-R (1)

Commanding General
U.S. Army Tank-Automotive Command
Warren, Michigan 48090

ATTN: AMSTA-RGD Mr. D. Wilburn (1)

Commander, U.S. Naval Weapons Center
China Lake, California 93555

ATTN: Code 408 Mr. Lawrence Nichols (1)

Commander, U.S. Naval Weapons Center
China Lake, California 93555

ATTN: Code 4056 Mr. E. E. Benton (1)

Commander, U.S. Naval Weapons Center
China Lake, California 93555

ATTN: Code 3533 Mr. Paul C. Driver (1)

Commander, U.S. Naval Weapons Center
China Lake, California 93555

ATTN: Code 4056/Mr. Fred E. Nicodemus (1)

Commander, U.S. Naval Missile Center
Point Mugu, California 93042

ATTN: Code 5353 Mr. James Karney (1)

Geography Programs
Office of Naval Research
Arlington, Virginia 22217

ATTN: Code 414 (1)

Commanding Officer, U.S. Naval Avionics Facility
21st Street and Arlington
Indianapolis, Indiana 46218

ATTN: 021/Mr. P. Brink (1)

Commanding Officer, U.S. Naval Avionics Facility
21st Street and Arlington
Indianapolis, Indiana 46218

ATTN: Division 811/Mr. W. Wuster (1)

U.S. Department of Agriculture
Agriculture Research Service
Soil and Water Conservation Research Division
Rio Grande Soil and Water Research Center
P.O. Box 267
Weslaco, Texas 78596

ATTN: Dr. William Allen (1)

NASA Scientific and Technical Information Facility
P.O. Box 33
College Park, Maryland 20740

ATTN: Acquisitions and Input Branch (1)

Spectrophotometry Group
Radiation Thermometry Section
Heat Division, IBS
National Bureau of Standards
Washington, D.C. 20234

ATTN: Mr. Victor R. Weidner (1)

Institute of Defense Analyses
400 Army-Navy Drive
Arlington, Virginia 22202

ATTN: Mr. Lucien Biberman (1)

Defense Documentation Center
Cameron Station
Alexandria, Virginia 22314

ATTN: TIPCR (12)

Vought Missiles and Space Company - Michigan
LTV Aerospace Corporation
P.O. Box 909
Warren, Michigan 48090 (1)

Water Resources System Section
Water and Land Resources Department
Water and Land Resources Department
Battell-Northwest
P.O. Box 999
Richland, Washington 99352

ATTN: Mr. Jay R. Ellason (1)

Texas Instruments Incorporated
13536 North Central Expressway
Dallas, Texas 75222

ATTN: Mail Station 381/Mr. Frank E. Kinsman (1)

Texas Instruments Incorporated
13536 North Central Expressway
Dallas, Texas 75222

ATTN: Mail Station 381/Dr. Dmetro Andrychuk (1)

Texas Instruments Incorporated
13510 North Central Expressway
Dallas, Texas 75222

ATTN: Mail Station 208/Dr. Guy S. Rambie (1)

Ohio State University
Electroscience Laboratory
1320 Kinnear Road
Columbus, Ohio 43212

ATTN: Mr. Robert A. Fouty (1)

Honeywell, Incorporated
Radiation Center
2 Forbes Road
Lexington, Massachusetts 02173

ATTN: Mail Station 42/Mr. G. J. Burrer (1)

Aerospace Corporation
P.O. Box 95085
Los Angeles, California 90045

ATTN: Mr. David Pierson (1)

Aerospace Corporation
P.O. Box 95085
Los Angeles, California 90045

ATTN: Mr. D. A. Lacer (1)

Thermophysical Properties Research Center
Purdue University, Research Park
2595 Yeager Road
West Lafayette, Indiana 47906 (1)

RACIC
Battelle Memorial Institute
505 King Avenue
Columbus, Ohio 43201 (1)

The University of Texas at Austin
Applied Research Laboratories
Aerospace Technology Division
P.O. Box 8029
10000 FM Road 1325
Austin, Texas 78713 (1)

Air Force Avionics Laboratory
Wright-Patterson Air Force Base, Ohio 45433

ATTN: AFAL/TEL/Mr. Richard Firsdon (1)

GTE Sylvania, Incorporated
Sylvania Electronic System - West
P.O. Box 205
Mountain View, California 94024

ATTN: Mr. Steven Roe (1)

General Dynamics
Electro-Dynamic Division
P.O. Box 127
3080 Pacific Highway
San Diego, California 92112

ATTN: Dr. J. V. Ravenis (1)

Commander, Naval Ordnance Laboratory
White Oak
Silver Spring, Maryland 20910

ATTN: Code 213/Mr. W. W. Talbert (1)

Commander, Naval Weapons Center
China Lake, California 93555

ATTN: Code 4062 Mr. H. P. Leet (1)

Technology Incorporated
7400 Colmel Glen Highway
Dayton, Ohio 45432

ATTN: Mr. W. S. Arnold (1)

NASA
Lewis Research Center
Cleveland, Ohio 44135

ATTN: Mr. Ronald J. Schertler (1)

4950 TTZDE
Wright-Patterson Air Force Base, Ohio 45433 (1)

2750th ABW/SSL
Wright-Patterson Air Force Base, Ohio 45433 (1)

Electro-Optical Systems
Xerox Corporation
300 N. Hampstead Street
Pasadena, California 91107

ATTN: Mr. Lee W. Carrier (1)

Hughes Research Laboratories
Division of Hughes Aircraft Company
3011 Malibu Canyon Road
Malibu, California 90265

ATTN: Mr. F. H. Tenney (1)

Willow Run Laboratories, Building 2041
Institute of Science and Technology
The University of Michigan
P.O. Box 618
Ann Arbor, Michigan 48107

ATTN: Mr. Howard Courtney (1)

Willow Run Laboratories, Building 2041
Institute of Science and Technology
The University of Michigan
P.O. Box 618
Ann Arbor, Michigan 48107

ATTN: Mr. Max E. Bair (1)

Willow Run Laboratories, Building 2041
Institute of Science and Technology
The University of Michigan
P.O. Box 618
Ann Arbor, Michigan 48107

ATTN: Mr. Richard Legault (1)

Willow Run Laboratories, Building 2041
Institute of Science and Technology
The University of Michigan
P.O. Box 618
Ann Arbor, Michigan 48107

ATTN: Infrared Information and Analysis Center (1)

UNCLASSIFIED

Security Classification

DOCUMENT CONTROL DATA - R & D

(Security classification of title, body of abstract and indexing annotation must be entered when the overall report is classified)

1. ORIGINATING ACTIVITY (Corporate author)	2a. REPORT SECURITY CLASSIFICATION
Willow Run Laboratories of the Institute of Science and Technology, The University of Michigan, Ann Arbor	UNCLASSIFIED
	2b. GROUP N/A

3. REPORT TITLE

TARGET SIGNATURE ANALYSIS CENTER: DATA COMPILATION—ELEVENTH SUPPLEMENT

4. DESCRIPTIVE NOTES (Type of report and inclusive dates)

Volume I. Bidirectional Reflectance: Definition, Discussion, and Utilization

5. AUTHOR(S) (First name, middle initial, last name)

Target Signature Analysis Center, Willow Run Laboratories

6. REPORT DATE	7a. TOTAL NO. OF PAGES	7b. NO. OF REFS
October 1972	vi + 57	9

8a. CONTRACT OR GRANT NO.	9a. ORIGINATOR'S REPORT NUMBER(S)
AF33(615)-70-C-1123	32210-41-B
b. PROJECT NO. 6239	
c.	9b. OTHER REPORT NO(S) (Any other numbers that may be assigned this report)
d.	AFAL-TR-72-226, Volume I

10. DISTRIBUTION STATEMENT

Approved for public release, distribution is unlimited.

11. SUPPLEMENTARY NOTES	12. SPONSORING MILITARY ACTIVITY
Volume I of two volumes	Air Force Avionics Laboratory Air Force Systems Command Wright-Patterson Air Force Base, Ohio

13. ABSTRACT

This report is the eleventh supplement to the Target Signature Analysis Center: Data Compilation and contains 2200 curves of bidirectional reflectance versus angle. The significance of this report to the Air Force is that these data provide the Air Force with essential optical properties-of-materials data to analyze the angular dependence of the reflected radiance from various targets. Volume I contains a definition of the parameters pertinent to the bidirectional reflectance, a discussion of the data, some equations for application of the data, and an index and cross reference of the data contained in Volume II. Bidirectional reflectance data are presented graphically in Volume II.

This supplement to the Target Signature Analysis Center: Data Compilation augments an ordered, indexed compilation of reflectance, radar cross sections, and apparent temperatures of target and background materials. The Data Compilation includes spectral reflectances and transmittances in the optical region from 0.3 to 15 μm, normalized radar cross sections, and apparent temperatures at mm wavelengths. When available, the experimental parameters associated with each curve are listed to provide the user with a description of the important experimental conditions.

DD FORM 1 NOV 65 1473

UNCLASSIFIED

Security Classification

KEY WORDS	LINK A		LINK B		LINK C	
	ROLE	WT	ROLE	WT	ROLE	WT
Data reduction O.D. paint specularity Reflectance standards Polarized bidirectional reflectance						